JOURNAL OF PETROLOGY | VOLUME 45 | NUMBER 8 | PAGES 1539–1564 | 2004 | DOI: 10.1093/petrology/egh015

Abundance and Partitioning of OH in a High-pressure Magmatic System: Megacrysts from the Monastery Kimberlite, South Africa

DAVID R. BELL[1]*, GEORGE R. ROSSMAN[1] AND RORY O. MOORE[2]

[1]DIVISION OF GEOLOGICAL AND PLANETARY SCIENCES, CALIFORNIA INSTITUTE OF TECHNOLOGY 170-25, PASADENA, CA 91125-2500, USA

[2]MINERAL SERVICES CANADA INC., 205–930 HARBOURSIDE DRIVE, NORTH VANCOUVER, B.C. V7P 3S7, CANADA

RECEIVED JULY 14, 2001; ACCEPTED DECEMBER 15, 2003
ADVANCE ACCESS PUBLICATION JULY 1, 2004

Concentrations of OH, and major and trace elements were determined in a suite of mantle-derived megacrysts that represent the crystallization products of a kimberlite-like magma at ~5 GPa and ~1400–1100°C. OH concentrations, determined by single-crystal Fourier transform infrared spectroscopy, display the following ranges (ppmw H_2O): olivine 54–262, orthopyroxene 215–263, garnet 15–74, clinopyroxene 195–620, and zircon 28–34. High OH concentrations in olivine imply mantle conditions of origin, with limited H loss during ascent. OH is consistently correlated with megacryst composition, exhibiting trends with Mg-number that are similar to those of other minor and trace elements and indicating a record of high-pressure magmatic evolution. H substitution is not coupled to minor elements in olivine, but may be in ortho- and clinopyroxene. The OH–Mg-number trends of garnet and clinopyroxene show inflections related to co-precipitation of ilmenite, suggesting minor element (Ti) influence on OH partitioning. During differentiation, relative OH enrichment in clinopyroxene and olivine is consistent with proportional dependence on water activity, whereas that in garnet suggests a higher power-law dependence and/or influence of temperature. Inter-mineral distribution coefficients for OH between cpx, opx, olivine and zircon are thus constant, whereas partitioning between these minerals and garnet shows a factor 4–10 variation, correlated regularly with composition (and temperature). Calculation of solid–melt partition coefficients for H at 5 GPa over a range of magmatic evolution from 1380 to 1250°C yields: ol 0·0053–0·0046, opx 0·0093–0·0059, cpx 0·016–0·013, gt 0·0014–0·0003, bulk (garnet lherzolite–melt) 0·0063–0·0051. These are consistent with experimental studies and similar to values inferred from mid-ocean ridge basalt geochemistry, confirming the moderate incompatibility of H in mantle melting.

KEY WORDS: *hydrogen; megacryst; mantle; trace element; water*

INTRODUCTION

There is now a substantial body of information indicating that OH is incorporated in trace but measurable amounts in the structure of most common minerals whose chemical formulae suggest that they are nominally anhydrous. OH occurring in this manner may constitute the dominant reservoir of H in the Earth's interior (Bell & Rossman, 1992*a*; Meade *et al.*, 1994; Smyth, 1994; Ingrin & Skogby, 2000), and is believed to play an important role in the physical properties of the mantle (Mackwell *et al.*, 1985; Karato, 1990; Hirth & Kohlstedt, 1996). This form of H may also influence the evolution of the hydrosphere through its behavior in mantle melting (Dixon *et al.*, 1988) and through the isotopic fractionation that may attend reactions involving this species (Bell & Ihinger, 2000). The basis for understanding these phenomena lies in quantitative knowledge of the partitioning behavior of H (and D) between various phases (minerals, melt, fluid) as a function of the various conditions relevant to the Earth's mantle.

Most studies to date on natural minerals have dealt with the infrared spectroscopic characteristics and abundance of OH in individual minerals, whereas relatively few (e.g. Rossman & Smyth, 1990; Beran *et al.*, 1993; Peslier *et al.*, 2002) have examined assemblages of coexisting minerals. Furthermore, there have been few (e.g. Arredondo *et al.*, 2001) attempts to use nominally anhydrous minerals in tracing the behavior of hydrous volatiles in igneous or metamorphic systems, despite the suggestion some two decades ago by Martin & Donnay (1972) that this could probably be done.

The experimental work necessary for extracting quantitative information about conditions and processes from

*Corresponding author. Present address: Department of Chemistry and Biochemistry, Arizona State University, Tempe, AZ 85287-1604, USA. Telephone: (480) 965-0163. Fax: (480) 965-2747. E-mail: David.R.Bell@asu.edu

the natural observations has received attention over the past decade (Geiger *et al.*, 1991; Bai & Kohlstedt, 1992, 1993; Kohlstedt *et al.*, 1996; Lu & Keppler, 1997; Withers *et al.*, 1998; Matveev *et al.*, 2001; Rauch & Keppler, 2002). These studies establish the relationship between OH in nominally anhydrous minerals and the fugacity of hydrous species with which the minerals have equilibrated at high pressures and temperatures. However, the complexities of natural geological systems require that these fundamental experimental investigations in simple chemical systems or under a limited range of conditions be complemented by studies on natural assemblages in order to be more useful in geology.

In this study, we examine in detail the relationship between OH content and other compositional features in a suite of co-magmatic megacryst minerals (garnet, olivine, orthopyroxene, clinopyroxene and zircon) from the Monastery kimberlite, South Africa. The compositional dependence of partitioning behavior of OH among high-pressure minerals is described and the relationship of the OH concentrations to water fugacity and concentration in the source is evaluated quantitatively with reference to the problems of hydrogen mobility under igneous conditions. These results complement high-pressure experimental studies in contributing to a foundation for understanding the behavior of hydrogen in the Earth's mantle.

THE MONASTERY MEGACRYST SUITE

Overview and significance of megacrysts

'Cr-poor megacrysts' (Eggler *et al.*, 1979) or 'discrete nodules' (Nixon & Boyd, 1973) are a common variety of mantle-derived xenolith sampled by kimberlite, characterized by large grain size and a distinctive range of chemical compositions. The wide range of compositions and temperatures recorded are consistent with megacrysts being differentiation products of a mantle-derived magma (Boyd & Nixon, 1973; Gurney *et al.*, 1979; Schulze, 1984, 1987). The composition of this magma, its physical setting and exact relationship to kimberlite, as erupted at the surface, are still under debate (Harte, 1983; Mitchell, 1986; Davies *et al.*, 2000). The ultra-coarse grain size and incompatible element enrichment evokes an analogy with crustal pegmatites, and an origin of the megacrysts in coarse veins and magmatic apophyses marginal to a partially molten diapir or magmatic intrusion has been proposed (Harte & Gurney, 1981). Analogous megacrysts in alnöites and alkali basalts are commonly considered to be broadly cognate with the host magmatic event (Irving, 1974; Schulze, 1987; Neal & Davidson, 1989) and a similar relationship of kimberlite megacrysts to their host is often proposed (e.g. Jones, 1987; Smith *et al.*, 1995).

Of relevance to this study are the observations (1) that these minerals record some of the highest pressures and temperatures encountered in mantle xenoliths, that temperatures span a wide and continuous range, but that pressure of origin is relatively restricted (Gurney *et al.*, 1979), and (2) that local chemical and isotopic equilibrium is a strong feature, unlike many peridotite xenoliths of both the low-temperature, granular, and high-temperature, sheared varieties.

Trace element concentrations in the minerals, and the kimberlite association inferred from isotopic studies (Jones, 1987; Nowell *et al.*, 1999), suggest that the megacryst parent magma was enriched in volatiles and incompatible trace elements. The Monastery megacrysts thus provide the opportunity to study in detail the behavior of H in mantle minerals under high P–T, equilibrium conditions in a hydrous mineral–melt system covering a range of chemical bulk compositions.

Chemical evolution of the Monastery megacryst suite

The large size, mineral diversity and great abundance of the megacryst suite at the Monastery kimberlite in the southeastern Free State, South Africa, has led to a number of studies on these samples, with the result that they represent one of the best documented kimberlite-hosted megacryst assemblages. The Monastery megacryst suite comprises olivine, garnet, clinopyroxene, orthopyroxene, ilmenite, phlogopite and zircon. Because these megacrysts commonly occur as isolated crystals, dispersed within the host kimberlite matrix, the petrological relationships of the minerals to one another are not immediately obvious and must be established by examination of (much rarer) samples where one or more minerals are intergrown. Detailed analysis of such relationships combined with extensive chemical analysis have revealed several associations of megacrysts, summarized in Table 1 (Gurney *et al.*, 1979, 1998; Moore *et al.*, 1992; Hatton, 1998). The relationships between these groups remain under investigation.

In the most easily understood group, referred to as the 'main silicate trend' (MST; Moore *et al.*, 1992; Gurney *et al.*, 1998), the studies of Jakob (1977), Gurney *et al.* (1979), Moore (1986) and Moore *et al.* (1992) show that crystallization begins with multiple saturation at the liquidus (~1400°C) with magnesian olivine (~Fo 88), orthopyroxene, garnet and highly subcalcic clinopyroxene [Ca/(Ca + Mg) ~0·3]. Pressure, determined on a rare four-phase peridotite with mineral compositions the same as the most primitive megacrysts, ranges from 4·5 to 6 GPa depending on choice of thermobarometer combination (Moore, 1986; D. R. Bell, unpublished data, 2003). At lower temperature (~1250°C), ilmenite (commonly in the form of lamellar pyroxene–ilmenite

Table 1: Megacryst paragenetic associations and mineral compositions

Megacryst group	Minerals	Compositional characteristics
Group 1	olivine	84 < Fo < 88; NiO > 0·2 wt %
'Main silicate trend'	orthopyroxene	Mg-number < 88; Ca-number > 0·5
(MST)	clinopyroxene	30 < Ca-number < 47
	garnet	66 < Mg-number < 80; TiO_2 > 0·5 wt %
	ilmenite	MgO 7–11 wt %; Cr_2O_3 < 0·5 wt %; Zr/Nb > 0·7
Group 2	olivine	77 < Fo < 83; NiO < 0·2 wt %
	phlogopite	84 < Mg-number < 87; 0·6 < TiO_2 < 1·3 wt %
	ilmenite	MgO < 10 wt %; Cr_2O_3 > 0·5 wt %; Zr/Nb <0·7
	zircon	
Group 3	clinopyroxene	Ca-number > 47
	phlogopite	87·5 < Mg-number < 91; 1·0 < TiO_2 < 1·6 wt %
	ilmenite	MgO > 11 wt %; Cr_2O_3 > 0·5 wt %; Zr/Nb <0·7
Lamellar enstatites	orthopyroxene	Mg-number > 88; Ca-number < 0·5
	cpx, gt (exsolved)	

intergrowths) replaces olivine in the sequence. Detailed study of coexisting mineral occurrences and geochemistry (Moore, 1986; Moore *et al.*, 1992; Gurney *et al.*, 1998; Hatton, 1998) has shown that no hydrous mineral (i.e. phlogopite) crystallizes together with these minerals. This group, or petrological association, forms the major focus of this study. The compositional relationships of the major silicates are shown in Fig. 1.

The other groups of megacrysts (groups 2 and 3; Moore *et al.*, 1992) include the minerals ilmenite, calcic clinopyroxene, Fe-rich olivine, phlogopite and zircon. Their relationship to the MST megacrysts was discussed by Moore *et al.* (1992), but does not affect the present study in a major way. In terms of the OH evolution of group 2 and 3 megacrysts, it is noteworthy that phlogopite appears to be a significant part of the assemblage over much of their evolution.

The bulk of this study focuses on the MST megacrysts. In addition, a suite of olivines belonging to the high-Fe (group 2) association has been analysed, together with zircon from this group. A single calcic clinopyroxene (group 3) was analysed.

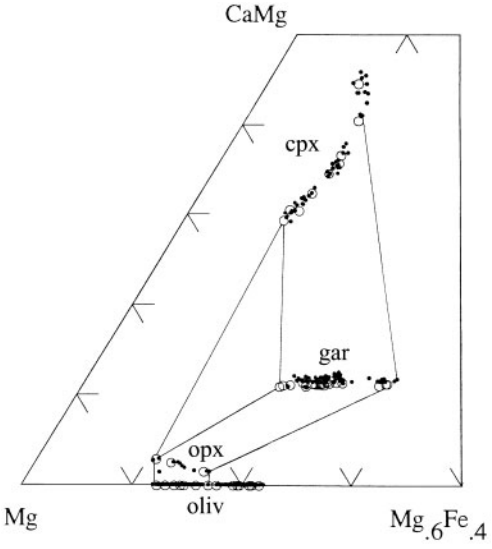

Fig. 1. Compositions of megacryst olivines, orthopyroxenes, garnets and clinopyroxenes from the Monastery kimberlite. Tie-lines indicate compositional relationships between the minerals. Highly calcic clinopyroxenes and Fe-rich olivines occupy compositions beyond the range of the 'main-trend' silicates and ilmenites (not shown). Small filled circles are analyses from Moore (1986) and unpublished data and represent extensive sampling ($n > 300$). Open circles are samples analysed for OH in this work, selected mostly from those previously analysed. Open circle compositions were determined at Caltech, with the exception of olivine (Geophysical Laboratory).

SAMPLES

Samples selected for this study were a subset of large collections previously studied by Moore (1986). Samples derive both from mine tailings dumps and from loose kimberlite boulders in the open pit and surrounding areas. Most come from a single phase of the intrusion (the Quarry kimberlite). The minerals for study were chosen on the basis of previously determined electron microprobe analyses (Moore, 1986 and unpublished data) to span the complete compositional range of each mineral observed for the large sample suites. This is illustrated in Fig. 1. For olivine, orthopyroxene and garnet the selection criterion was 100Mg/(Mg + Fe) (Mg-number), whereas clinopyroxene samples were chosen on

Table 2: Polarizations summed and calibrations used in determining OH contents (as ppm H_2O by weight) of minerals in this study

Mineral	Polarizations summed	Calibration used	Integrated molar absorption coefficient (l/mol per cm^2)
Garnet	$A = A$ (unpol.)	ppm $H_2O = 0{\cdot}719A/cm$	6700[1]
Olivine	$A = A_\beta + A_\gamma$	ppm $H_2O = 0{\cdot}233A/cm$	22740[2]
Clinopyroxene	$A = A_\alpha + A_\beta + A_\gamma$	ppm $H_2O = 0{\cdot}141A/cm$	38300[1]
Orthopyroxene	$A = A_\alpha + A_\beta + A_\gamma$	ppm $H_2O = 0{\cdot}0674A/cm$	80600[1]
Zircon	$A = A_{//c} + 2A_{//a}$	ppm $H_2O = 1{\cdot}04A/cm$	4740[3]

[1]Bell *et al.* (1995*b*). [2]Bell *et al.* (2003) (but see text). [3]D. Bell, G. Rossman, D. Endisch, J. Maldener & F. Rauch (unpublished data).

the basis of 100Ca/(Ca + Mg) (Ca-number), a temperature index that is also well correlated with Mg-number in this mineral. Zircon samples were all from bi- or polymineralic intergrowths and were chosen on the basis of the Mg-number of the coexisting olivine or ilmenite. Original grain sizes for the monomineralic megacrysts, excluding olivine, ranged from 2 to 15 cm, whereas intergrowths occur more typically on the scale of millimeters to 1 cm.

OH contents of coexisting minerals were determined on one pair each of garnet–clinopyroxene, garnet–olivine and olivine–zircon. In addition, the OH contents of three clinopyroxene samples coexisting with ilmenite in the form of lamellar intergrowths were determined.

METHODS

Infrared spectroscopy

Our procedure for quantitative IR spectroscopic analysis of minerals, described by Bell & Rossman (1992*a*, 1992*b*) and Bell *et al.* (1995*b*), uses doubly polished plates prepared in the appropriate crystallographic orientation from large, clear fragments handpicked from coarsely crushed pieces of megacryst. For the optically biaxial minerals, more than one grain was often required to generate spectra polarized in all three principal vibration directions of the optical indicatrix. For the isotropic garnets, analyses were based on an unpolarized measurement performed in random crystallographic orientation. Degree of homogeneity in OH content of the Monastery olivines was investigated by the analysis of multiple spots within individual grains and by analysis of multiple and petrographically different subgrains from individual 'megacrysts'.

All OH concentrations were derived from integrated intensities of the OH absorptions from 4000 to 2800 cm^{-1}, using the molar absorption coefficients given in Table 2. We estimate that the uncertainty (95% confidence level) in the integrated absorbances and, therefore, in the relative OH concentrations, is approximately 10% for garnet, pyroxenes and zircon and 15% for olivine. The higher uncertainty in olivine derives from variable contribution of molecular water OH (see below), which cannot be unambiguously resolved, and also the generally lower signal-to-noise ratio of olivine spectra caused by internal absorption and scattering of light owing to microscopic imperfections. Absolute accuracy of the OH concentrations varies according to precision and accuracy of the calibration method for the individual minerals and depends on consistent choice of baseline. For each mineral, it may also depend on the precise features of the OH absorption spectra, which are generally not constant and depend on mineral composition. These quantitative issues have been discussed further by Bell *et al.* (1995*b*, 2003). In the present case, these uncertainties in the molar absorptivity are expected to be minor and, in the absence of more precise information, have been ignored in calculation of OH concentrations.

Bell *et al.* (2003) presented a calibration of OH in olivine that differed substantially from the widely used previous calibration of Paterson (1982). The olivine OH concentrations determined here are based upon the results and methods of Bell *et al.* (2003), but were calculated from the summed integrated absorbances in the β and γ polarizations only, because the low absorption in the α polarization was considered to introduce unwarranted uncertainty.

In all tables and figures, the OH concentrations are expressed as parts per million H_2O by weight. This does not carry the implication of water molecules within the mineral structure, but follows the common convention of expressing mineral analyses in terms of weight fraction of an oxide component appropriate to the assumed cationic charge (H = +1). In the text, we refer to the hydrous component as OH. Strictly speaking, this could include

water molecules (which have hydroxyl groups) as well as hydroxide in the mineral structure. However, unless indicated to the contrary, the term OH generally refers here to hydroxide (hydroxyl) bound in the mineral structure. The symbol H denotes the element hydrogen, irrespective of chemical species.

Electron microprobe

Initial wavelength-dispersive electron microprobe analyses for sample selection were performed on a Cameca Camebax instrument at the University of Cape Town (UCT), operating at 15 kV. Data processing followed the PAP method (Pouchou & Pichoir, 1991) used by Cameca. Garnets and pyroxenes were reanalyzed at Caltech on a JEOL 733 instrument, operated at 15 and 20 kV accelerating voltage and beam currents from 30 to 500 nA (measured on a Faraday Cup) depending on element abundances. Olivine trace element analyses were performed on a JEOL-JXA-8900 microprobe at the Geophysical Laboratory, Carnegie Institution of Washington (GL), operating at 20 kV and 300 nA. In addition to the high beam currents, extended counting times up to 4 min on both peak and background were used for low abundance elements in all minerals. Detection limits (approximated as $3\sigma_B$) are in the range 10–30 ppm. Corresponding counting statistic errors for individual trace element analyses with >100 ppm concentration levels are typically less than 10% relative. Data reduction for both JEOL instruments was by the CITZAF method of Armstrong (1988, 1991). Analyses were performed on multiple grains picked from crushed samples. In general, good agreement in major element concentration was found between the laboratories, although a difference in Mg-number of ~0·7 was noted between the UCT and GL olivine analyses. This is a confirmation of both analytical accuracy, to the extent that it is required for establishing the compositional trends, as well as mineral homogeneity, because the analyses were carried out on different grains from the same sample.

RESULTS

Petrography and microstructure of olivine

Olivine megacrysts occur as large, fractured and partially serpentinized masses, up to ~10 cm in size, embedded in kimberlite matrix, from which they are commonly liberated by mining and processing procedures. Some 'megacryst' olivines show evidence of recrystallization, to the extent that they may more accurately be termed porphyroclastic dunites. Such samples comprise variable proportions of large, often strained porphyroclasts, small (sub-millimeter) neoblasts and euhedral recrystallized tablets. They are visually heterogeneous from one grain of the polycrystalline aggregate to another, as well as within individual grains, where a variety of dislocations, tilt walls, microfaults, healed fractures and inclusions may be present in individual aggregates. Many of the features, both in terms of mineral habit and fabric, and internal mineral microstructure are identical to those seen in olivines from high-temperature deformed lherzolites (Boullier & Nicolas, 1973, 1975; Gueguen, 1977, 1979; Drury & Van Roermund, 1988, 1989) and in Fe-rich dunites and peridotites from the Kimberley pipes (Dawson *et al.*, 1981). Noting that any of these structures might be accompanied by OH groups or H_2O molecules, the petrographic features visible with the optical microscope to a magnification of 400× of each sample analysed have been recorded (Table 3).

A consistent difference in appearance was noted between the two chemical groups of olivines. At 400× in transmitted light, the low-Fe olivines had a pervasive and relatively uniform fine 'granular' appearance, indicating the presence of structural heterogeneities at the limit of optical resolution. In contrast, the high-Fe group were optically homogeneous under these conditions of examination.

Characteristics of OH spectra

Representative mineral spectra are illustrated in Fig. 2a–e. In general, these are similar to previously published spectra of OH in mantle minerals.

Garnets

The garnet spectra (Fig. 2a) are typical of OH in kimberlite megacrysts (Bell & Rossman, 1992*b*; Matsyuk *et al.*, 1998). The spectra show a regular composition-dependent change in shape, which is discussed further, with reference to compositional dependence of OH partitioning involving garnet, in a later section.

Pyroxenes

Clinopyroxene and orthopyroxene spectra (Fig. 2b and Fig. 2c, respectively) are generally similar to those described by Skogby *et al.* (1990), and show some composition-dependent variability. Most obvious is a change in the relative proportions of the 3600 cm^{-1} and 3540 cm^{-1} bands in the clinopyroxene spectrum, which increase and decrease respectively with increasing compositional evolution (higher Ca-number).

Olivine

Olivine IR OH spectra are similar to those previously reported by Miller *et al.* (1987), but whereas that study described a large number of different types of spectra, the spectra of samples studied here are relatively uniform. However, the two compositional groupings of olivines have OH spectra that are consistently different. As

Table 3: Spectroscopic, compositional and petrographic details of individual olivine samples

Sample	Fo (UCT)	Spectroscopic		OH abundance		Conditions		Microscopic petrographic features				
		Pol.	ΣIA[1]	NRA[2] (ppm)	Paterson[3] (H/10^6 Si)	f_{H_2O}[4] (GPa)	a_{H_2O}[5]	A	B	C	D	E
Low-Fe, high-Ni olivines												
MON24-OL1.B	85·6	β + γ	671·5	156	770	40·4	0·109				not examined	
MON24-OL2.B	85·6	β + γ	543·8	127	624	32·7	0·088				not examined	
ROM250-OL2.1	84·2	β + γ	783·4	182	875	44·8	0·121	1	2	0	0	scattered, 1–4 μm
ROM250-OL2.2	84·2	α + β	389·9	184	411	19·7	0·053	1	0	2	0	2–10 μm, lilypads
ROM250-OL16.1	83·1	β + γ	728·2	170	836	43·6	0·118	1	0	0	0	0
ROM250-OL16.2	83·1	β	229·7	198	243	11·3	0·030	1	0	0	H	1
ROM250-OL24.1	85·3	β + γ	560·0	130	625	32·4	0·088	1	0	0	0	0
ROM250-OL29.1	86·2	β + γ	881·2	205	937	44·7	0·121	1	0	2	0	0
ROM250-OL42.1	87·0	β + γ	686·3	160	769	39·2	0·106	?	2	1	2	0
ROM250-OL42.2	87·0	β + γ	338·3	79	362	17·6	0·048	1	tr	tr	0	0
ROM250-OL42·3	87·0	β + γ	232·6	54	250	11·9	0·032	0	0	0	healed	1 μm
ROM250-OL54.1	87·8	β + γ	651·2	152	708	35·2	0·095	1	1	0	1	0
ROM250-OL54.2	87·8	β + γ	675·5	157	733	35·7	0·097	1	0	0	0	0
ROM250-OL54.3	87·8	β + γ	694·0	162	764	39·2	0·106	1	0	1	1	1 μm
ROM250-OL54.5	87·8	β + γ	608·1	142	678	35·2	0·095	1	tr, H.	1	0	0
High-Fe, low-Ni olivines												
ROM250-OL13.1A	79·1	β + γ	1085·6	253	1351	72·4	0·196	0	2	0	1	1 μm (2)
ROM250-OL13.1B	79·1	β + γ	1016·4	237	1267	68·2	0·185	0	2	0	1	1 μm (2)
ROM250-OL13.1C	79·1	β + γ	1038·2	242	1307	71·0	0·192	0	2	0	1	1 μm (2)
ROM250-OL13.1D	79·1	β + γ	1028·3	239	1310	71·9	0·195	0	2	0	1	1 μm (2)
ROM250-OL13.2	79·1	β + γ	1077·8	251	1303	68·1	0·184	0	0	1	0	2
ROM250-OL21.1	82·3	β	193·1	166	224	11·7	0·032	0	0	0	0	tr
ROM250-OL26.1	80·2	β + α	318·0	150	336	15·8	0·043	0	1	0	2	?
ROM250-OL26.2	80·2	β + γ	1124·3	262	1338	70·8	0·192	0	0	0	0	?
ROM250-OL40.1	78·4	β + γ	194·7	45	270	15·5	0·042	0	0	0	0	0
ROM250-OL40.	78·4	β + γ	363·0	85	487	26·9	0·073	0	1(L)	0	2	?
ROM177-OL	80·8	β + γ	535·0	125	668	35·6	0·096	0	0	0	1(L)	1–3 μm (2)
ROM181.OL1	79·3	β + γ	522·3	122	698	39·0	0·106	0	0	0	2	1–3 μm (2)
ROM181.OL2	79·3	β + γ	362·0	84	470	25·6	0·069	0	0	0	0	1, but many 2° incls
ROM121-Z010.OL1	80·4	α + γ	347·9	85	482	27·3	0·074	0	0	0	0	tr

[1]Summed integrated absorbance of the indicated polarizations per centimeter sample thickness, with contribution from serpentine removed.
[2]H_2O as ppm by weight determined by NRA calibration (Bell *et al.*, 2003).
[3]H_2O as H/10^6 Si, determined by the calibration of Paterson (1982) (note: 2 and 3 differ by about ×3).
[4]Calculated from the work of Kohlstedt *et al.* (1996).
[5]Defined as $f_{H_2O}/f^0_{H_2O}$, where the denominator is the fugacity of pure water at 5·2 GPa and 1300°C, calculated according to Saxena & Fei (1987).
Microscopic petrographic categories: A, background 'granularity', referring to fine-scale granular feature not resolvable at 400×. B, Parallelipipedic cells (Gueguen, 1979). C, Geometrically necessary dislocations (Gueguen, 1979). D, Microfaults or 'shear zones', referring to disruptions to the crystal in the form of ragged cracks, often running diagonally through the parallelepipedic structure defined by the tilt walls. Commonly discolored to a darker hue. E, Inclusions, referring to primary, often euhedral inclusions, not obviously associated with healed fractures. 0, absent; tr, trace; 1, present; 2, abundant; L, large; H, heterogeneously distributed.

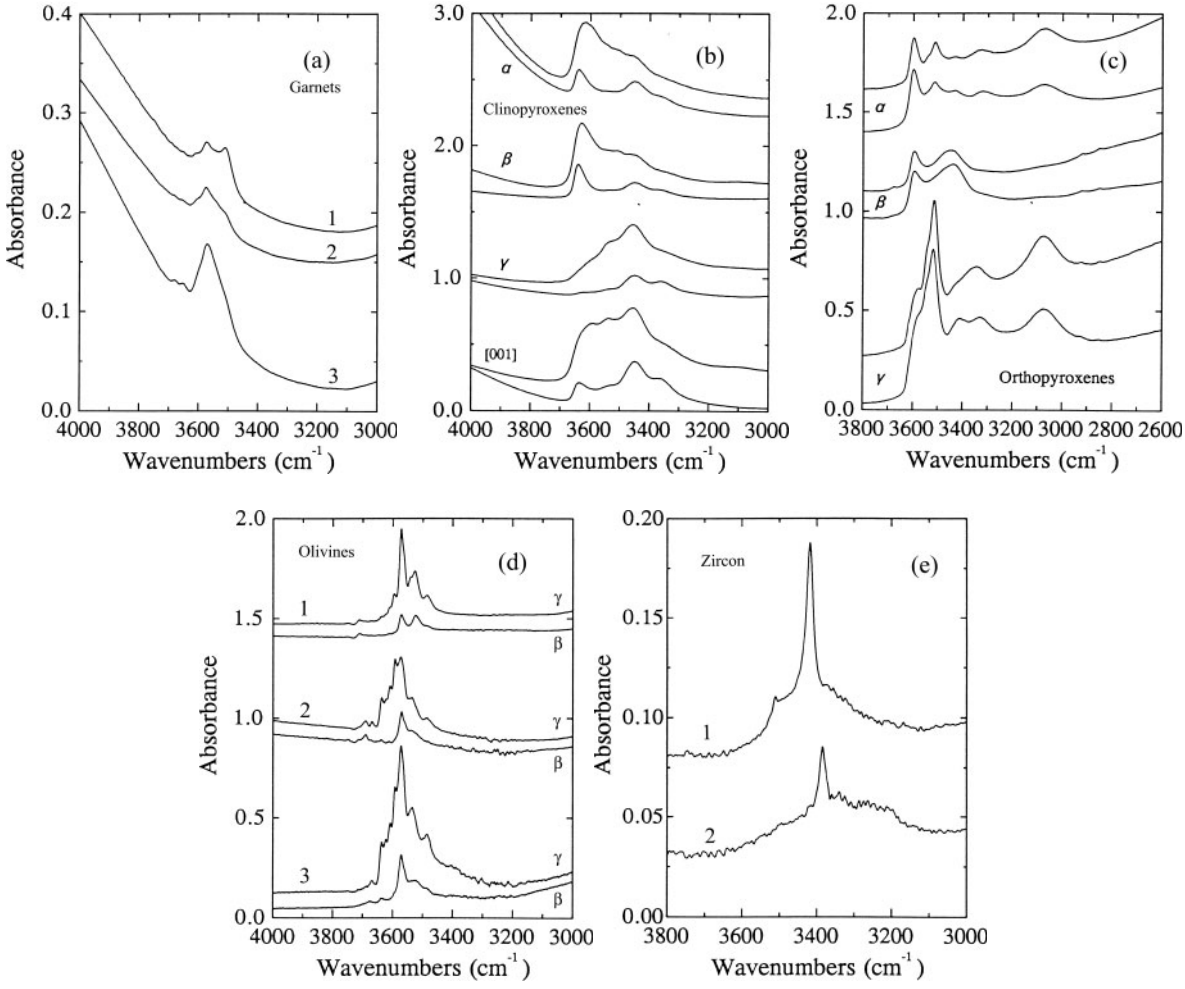

Fig. 2. Infrared spectra of megacryst minerals normalized to 1 mm thickness. (a) Garnets, unpolarized, showing change in proportions of bands near 3750 and 3512 cm^{-1}; (1) ROM263-GT09; (2) ROM263-GT25; (3) ROM263-GT36. (b) Clinopyroxenes, polarized parallel to α, β [010], γ and c [001]. The upper spectrum in each polarization is sample ROM271-DI16 and the lower spectrum sample ROM271-DI10. (c) Orthopyroxenes, polarized parallel to α [001], β [010] and γ [100]. The upper spectrum in each polarization is sample ROM273-OG1 and the lower spectrum is sample ROM167. (d) Olivine, polarized parallel to γ [100] (upper spectra) and β [001] (lower spectra). (1) Typical spectrum of olivine from the magnesian 'main silicate trend' group [ROM250-OL24]. (2) and (3) are spectra of high-Fe olivines of the type associated with ilmenite, phlogopite and zircon: (2) ROM121-Z010 and (3) ROM250-OL13. (e) Zircon ROM177.Z1, polarized parallel (upper spectrum; 1) and perpendicular (lower spectrum; 2) to *c*.

noted by Miller *et al.* (1987) for most olivines, these samples exhibit by far the strongest absorption for IR radiation polarized with **E** || [100] (i.e. γ), with absorption intensity for most bands decreasing in the order [100] (γ) > [001] (β) > [010] (α). This emphasizes the need for consistent orientation of olivine samples for comparative studies. Typical spectra from each of the two compositional groups of olivines are shown in Fig. 2d.

In the spectra of both compositional groups of olivine and in both the [100] and [001] polarization directions, the most intense band occurs at 3572 ± 2 cm^{-1}. Its frequency is independent of composition, as appears to be the case for most bands from the data at hand. The intensity of the 3572 cm^{-1} band in the [100] polarization direction is well correlated with total integrated OH absorbance and could therefore also be used as a crude indication of the total OH concentration in these samples.

Notable differences between the spectra of the two compositional groups include the enhanced intensity of bands on the high-frequency side of this main band in the more Fe-rich olivines ([100] polarization) and reduced intensity of the 3526 cm^{-1} band, relative to the main 3572 cm^{-1} band, in the Fe-rich olivines ([001] polarization). Both groups of spectra indicate the possibility of some molecular water in the samples (manifested by a broad band centered near 3420 cm^{-1}), but this is difficult to quantify unambiguously because of overlap with the

mineral OH bands. In calculation of the integrated absorbances and resultant H_2O contents of Table 3, it has been attempted to screen out this component by estimating its abundance from the [100] spectra. This possible molecular water may occupy the micro-cracks that pervade many of the samples, or may be associated with the minute inclusions described above.

Zircon

The zircon spectra (Fig. 2e) are very similar to that of sample 1229 from Kimberley (Woodhead *et al.*, 1991), consisting of two sharp pleochroic bands superimposed on a small amount of broad, featureless absorption. Upon heating to 400°C, much of this broader component is incorporated into the sharper bands, suggesting that it may have originally been bound in the zircon structure. This behavior has previously been reported by Woodhead *et al.* (1991).

OH concentrations

Tables 3–5 list the OH concentrations, expressed as ppm H_2O by weight (the usage throughout this paper) for the Monastery megacryst minerals. The relative abundances of OH are similar to those observed in these minerals from other mantle environments and concentrations fall within the ranges previously defined for these minerals from the mantle (Bell & Rossman, 1992*a*, 1992*b*; Kurosawa *et al.*, 1993; Snyder *et al.*, 1995; Matsyuk *et al.*, 1998; Peslier *et al.*, 2002), decreasing in the order clinopyroxene (291–620 ppm) > orthopyroxene (215–263 ppm) > olivine (43–245 ppm) > garnet (15–74 ppm) > zircon (28–34 ppm). Multiple analysis of the megacrysts used in calibration studies has revealed homogeneity (Bell *et al.*, 1995*b*). Here, general intra-crystalline homogeneity of megacrysts is supported by our occasional multiple analyses. This is generally, but not rigorously, true of other elemental concentrations in megacrysts (except for edge effects related to reaction with host kimberlite liquids). A notable exception is the variability in OH observed between different textural domains in a deformed and annealed olivine sample ROM250-OL42, discussed below.

For zircon, the range in concentration determined on two grains from the same sample is greater than that observed between all three samples and is approximately at the limit of analytical precision, i.e. the total variation observed could be caused by analytical uncertainties.

OH variability in olivine and petrographic correlations

OH concentrations in these megacrysts constitute the highest values measured in mantle olivines, consistent with the hypothesis that they crystallized from a magma or fluid enriched in volatiles and incompatible elements at high pressure. High OH in olivine is also favoured (Wright & Catlow, 1994) by the high Fe^{3+} environment of these samples (Bell & Mattioli, 1994). With the exception of a rare boron-bearing olivine from Tayozhnoye, Siberia (Sykes *et al.*, 1994), similar concentrations have been previously found only in samples derived from kimberlites.

Analysis of different subgrains from the same 'megacryst' reveals both homogeneity and heterogeneity. Four spots in a single grain (13.1) from sample ROM250-OL13 are identical in OH content within uncertainty of measurement and are also indistinguishable from a second grain (13.2) with different internal structure from the same 'megacryst'. Although these samples are petrographically different, all contain features indicating deformation. In another sample (ROM250-OL54), slight heterogeneity (~15%) was seen among four oriented cubes. This is slightly greater than the heterogeneity that might be expected from crystallographic misalignment, but could not be correlated with any visible (or other chemical) feature.

In contrast, petrographically different grains from ROM250-OL42 have significantly different OH contents. A highly strained porphyroclast traversed by shear fractures (OL42.1) has OH content similar to other megacrysts whereas two euhedral tablets (OL42.2, OL42.3) that appear to have recrystallized and annealed, although still showing some traces of relic deformation features, have much lower OH contents (Fig. 3). Annealed grains in other samples do not show this dramatic reduction in OH content, and it appears that, in general, there is little relationship of the OH content to grain microstructure or inclusion content. There is little variation in other chemical components between porphyroclasts and recrystallized neoblasts or tablets in these samples, making chemical origins for the OH differences unlikely. For this reason we suggest that the lower OH content of the OL42 tablets may be due to their annealing during ascent or emplacement of the kimberlite (Mercier, 1979) when water pressures are likely to be reduced from those in their mantle source.

Water fugacities and the preservation of mantle-derived OH in olivine

Because of the high diffusion rates measured for hydrous components in olivines (Mackwell & Kohlstedt, 1990; Kohlstedt & Mackwell, 1998, 1999), pyroxenes (Ingrin *et al.*, 1995; Hercule & Ingrin, 1999; Carpenter *et al.*, 2000) and garnets (Wang *et al.*, 1996), it has commonly been asserted that the measured levels of OH in mantle-derived minerals bear little relation to those in the source region. Although such inference appears to be a logical conclusion drawn from sound observations, the evidence from natural samples presented below suggests otherwise.

Table 4: Compositions of garnets, clinopyroxenes and orthopyroxenes

Sample	Na_2O	MgO	Al_2O_3	SiO_2	P (ppm)	K (ppm)	CaO	Sc (ppm)	TiO_2	V (ppm)	Cr_2O_3	MnO	FeO*	Ni (ppm)	Zr (ppm)	H_2O (ppm)	Total	Differentiation Index
Garnets																		Mg-no.
ROM263-GT02	0·099	19·34	21·30	41·47	173	n.a.	4·50	87	1·15	234	0·542	0·27	11·09	91	106	46	99·83	75·7
ROM263-GT03	0·110	19·40	20·90	42·32	164	n.a.	4·47	86	1·10	236	0·483	0·27	11·38	84	104	40	100·51	75·2
ROM263-GT04	0·112	19·24	20·55	41·91	169	n.a.	4·57	87	1·22	231	0·524	0·27	11·56	83	120	52	100·05	74·8
ROM263-GT06	0·107	19·79	20·92	42·36	201	n.a.	4·56	88	1·19	222	0·620	0·26	10·82	114	130	33	100·72	76·5
ROM263-GT09	0·102	19·26	21·21	41·53	159	n.a.	4·54	86	1·18	243	0·571	0·27	11·24	84	115	40	99·98	75·3
ROM263-GT10	0·115	19·06	20·89	41·99	185	n.a.	4·60	85	1·22	235	0·479	0·28	11·86	87	114	57	100·56	74·1
ROM263-GT25	0·093	19·94	21·05	41·85	194	n.a.	4·60	90	1·15	218	0·769	0·25	10·28	117	111	32	100·07	77·6
ROM263-GT31	0·105	19·27	20·49	41·82	154	n.a.	4·60	91	1·25	239	0·568	0·28	11·38	84	131	53	99·86	75·1
ROM263-GT34	0·092	17·74	21·29	41·53	167	n.a.	4·39	115	0·72	151	0·006	0·40	13·77	9	219	57	100·02	69·7
ROM263-GT36	0·084	17·49	21·60	41·12	194	n.a.	4·47	125	0·75	169	0·009	0·40	14·09	4	259	74	100·12	68·9
ROM263-GT44	0·094	20·39	20·59	41·97	197	n.a.	4·51	92	1·11	194	0·864	0·22	9·79	129	132	19	99·64	78·8
ROM263-GT49	0·104	18·72	21·52	41·42	195	n.a.	4·54	94	1·13	231	0·207	0·32	12·04	56	148	60	100·10	73·5
ROM263-GT52	0·093	20·61	21·11	41·97	172	n.a.	4·41	85	0·99	191	1·012	0·23	9·30	141	100	15	99·81	79·8
ROM263-GT68	0·100	19·52	20·73	41·91	168	n.a.	4·49	88	1·17	211	0·560	0·28	10·91	104	105	43	99·75	76·1
ROM263-GT71	0·083	17·40	21·88	41·07	178	n.a.	4·44	119	0·71	170	0·014	0·39	13·91	5	226	59	99·99	69·0
ROM263-GT75	0·107	19·43	20·66	41·86	175	n.a.	4·50	92	1·16	219	0·547	0·27	11·11	93	99	47	99·72	75·7
MON-9	0·106	19·09	20·92	41·25	178	n.a.	4·67	90	1·30	250	0·620	0·28	11·17	96	128	56	99·42	75·3
MON-24[1]	0·098	20·24	21·39	42·08	n.a.	n.a.	4·50	n.a.	1·05	n.a.	0·677	0·28	10·71	n.a.	n.a.	35	101·01	77·1
MON-26[2]	0·096	20·86	21·27	42·05	n.a.	n.a.	4·53	86	1·09	171	1·063	0·25	9·58	151	101	16	100·79	79·5
Clinopyroxenes																		Ca-no.
ROM273-DI10	1·29	16·20	0·55	55·32	n.a.	38	21·35	n.a.	0·143	289	0·296	0·10	5·08	63	n.a.	195	100·37	48·6
ROM273-DI16	1·54	20·78	2·46	55·82	n.a.	195	13·78	n.a.	0·330	120	0·301	0·12	5·51	674	n.a.	439	100·77	32·3
ROM273-DI21	1·78	19·02	2·54	55·09	n.a.	201	14·93	n.a.	0·486	188	0·196	0·13	6·04	457	n.a.	490	100·33	36·1
ROM273-DI24	2·10	15·94	2·45	54·87	n.a.	126	18·30	n.a.	0·255	194	0·242	0·12	5·98	172	n.a.	291	100·32	45·2
ROM387	1·71	19·87	2·60	55·86	n.a.	187	14·10	n.a.	0·403	157	0·210	0·15	5·98	572	n.a.	501	100·98	33·8
ROM270-CI11[3]	1·81	18·16	2·46	55·49	n.a.	194	15·94	n.a.	0·473	208	0·060	0·13	6·29	305	n.a.	554	100·91	38·7
ROM270-CI25[3]	1·88	17·29	2·42	55·38	n.a.	171	16·76	n.a.	0·363	188	0·008	0·14	6·28	124	n.a.	448	100·59	41·0
MON-25[3]	1·94	17·49	2·54	55·50	n.a.	167	16·33	n.a.	0·408	192	0·014	0·14	6·42	151	n.a.	469	100·85	40·2
MON-26[4]	1·60	20·25	2·45	55·85	n.a.	264	14·26	n.a.	0·391	148	0·305	0·13	5·44	662	n.a.	620	100·81	33·6
Orthopyroxenes																		Mg-no.
ROM273-OG1	0·28	32·30	1·14	57·30	n.a.	n.a.	1·34	n.a.	0·258	n.a.	0·07	0·10	8·29	n.a.	n.a.	251	101·09	87·4
ROM273-OG2	0·31	32·60	1·29	57·37	n.a.	n.a.	1·52	n.a.	0·209	n.a.	0·13	0·13	7·20	n.a.	n.a.	263	100·75	89·0
ROM-167	0·18	31·31	0·72	56·96	n.a.	n.a.	0·8	n.a.	0·156	n.a.	0	0·18	10·64	n.a.	n.a.	215	100·94	84·0

[1]Coexists with olivine. [2]Coexists with cpx. [3]Coexists with ilmenite. [4]Coexists with garnet. n.a., not analyzed.

Table 5: Compositions of olivine megacrysts and megacryst intergrowths

Sample	Assemblage	SiO_2	TiO_2	Al_2O_3	Cr_2O_3	FeO	MnO	MgO	CaO	Na_2O	P_2O_5	NiO	H_2Ool	H_2Ozir	Mg-no.
Low-Fe, high-Ni group ('Main silicate trend')															
ROM250-OL02	ol	39·16	0·040	0·033	0·006	14·44	0·126	46·01	0·080	0·028	0·015	0·307	183	—	85·03
ROM250-OL16	ol	39·14	0·046	0·028	0·004	15·33	0·130	45·53	0·068	0·026	0·014	0·243	170	—	84·11
ROM250-OL24	ol	39·45	0·035	0·038	0·011	13·50	0·119	46·69	0·087	0·030	0·016	0·352	130	—	86·04
ROM250-OL29	ol	39·50	0·032	0·042	0·015	12·85	0·118	47·23	0·092	0·037	0·016	0·375	205	—	86·76
ROM250-OL42.a	ol	39·54	0·031	0·048	0·019	12·33	0·116	47·53	0·098	0·032	0·017	0·389	160	—	87·30
ROM250-OL42.b	ol	39·70	0·032	0·049	0·019	12·29	0·114	47·61	0·097	0·033	0·015	0·384	79	—	87·35
ROM250-OL42.c	ol	39·67	0·030	0·047	0·017	12·31	0·114	47·50	0·103	0·030	0·015	0·383	54	—	87·31
ROM250-OL54	ol	39·62	0·032	0·048	0·017	12·28	0·113	47·54	0·095	0·033	0·015	0·384	153	—	87·34
MON-24	ol–gt	39·60	0·039	0·035	0·009	13·70	0·123	46·93	0·081	0·031	0·016	0·348	156*	—	85·93
High-Fe, low-Ni group															
ROM250-OL13	ol	38·61	0·018	0·001	0·002	19·09	0·202	42·84	0·046	0·009	0·017	0·066	244	—	80·00
ROM250-OL21	ol	39·18	0·023	0·001	0·007	15·85	0·171	45·52	0·044	0·011	0·024	0·106	166	—	83·66
ROM250-OL26	ol	38·84	0·024	0·004	0·003	17·85	0·171	43·94	0·047	0·011	0·014	0·135	262	—	81·44
ROM250-OL40	ol	38·67	0·017	0·001	0·001	19·26	0·200	42·76	0·045	0·010	0·019	0·058	85*	—	79·83
MON-14	ol–ilm	39·02	0·021	0·006	0·005	17·31	0·183	44·32	0·029	0·011	0·017	0·085	n.a.	—	82·03
ROM009	ol–ilm	38·89	0·022	n.d.	0·003	17·59	0·182	44·07	0·043	0·012	0·021	0·087	n.a.	—	81·71
ROM177	ol–zir	38·87	0·020	0·001	0·002	17·71	0·180	43·93	0·044	0·012	0·020	0·086	125	34	81·56
ROM181	ol–zir	38·55	0·023	0·003	0·003	18·93	0·173	42·68	0·048	0·015	0·015	0·117	122*	33*	80·08
ROM121-Z010	ol–ilm–zir	38·85	0·021	0·002	0·002	17·74	0·186	43·68	0·044	0·013	0·019	0·078	85	28	81·44

n.a., not analyzed; n.d., not detected.
*The higher of two discrepant analyses (see Table 2, Fig. 3).

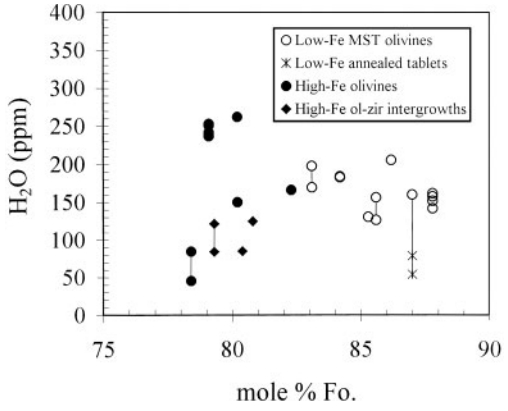

Fig. 3. OH content of olivine, expressed as ppm H_2O by weight, as a function of mole % forsterite component. Points joined by vertical lines are analyses of different spots in the same sample. Star symbols represent annealed euhedral tablets within deformed olivine porphyroclasts.

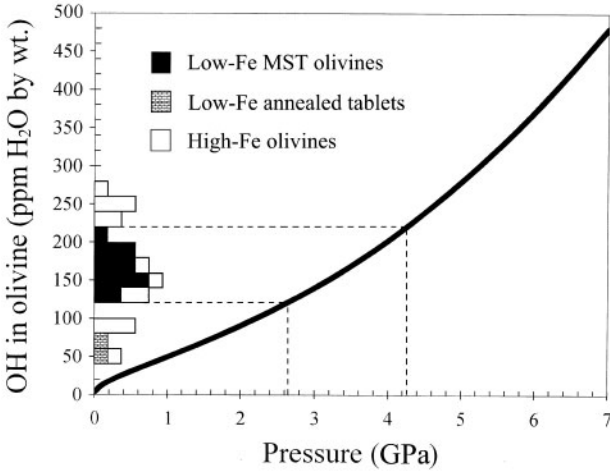

Fig. 4. Diagram illustrating the minimum pressure of origin of the hydrous component in the olivine samples of this study. The bold line represents the 'solubility' of OH in olivine as a function of pressure as determined experimentally by Kohlstedt *et al.* (1996), but modified in an attempt to reconcile differences in the analytical methods used to determine OH in olivine between that and the present study. The OH contents of the samples in this study are shown in histogram form on the ordinate. Dashed lines indicate the range of minimum pressures of origin indicated by the measured OH contents for the low-Fe (MST) olivine megacrysts (filled bars). In that these minimum pressures are calculated on the assumption that $P_{H_2O} = P_{total}$, the petrological unlikelihood of such high water activity strongly suggests higher pressures of origin consistent with mineral thermobarometry of low-Fe olivine megacryst assemblages.

Bai & Kohlstedt (1992) and Kohlstedt *et al.* (1996) determined the OH content of olivine saturated with a pure water fluid phase at pressures from 0·05 to 13 GPa. This saturation curve, representing the 'solubility' of H in olivine, is shown in Fig. 4, along with the measured concentrations from this study reported in Tables 3 and 5. This figure demonstrates that, apart from tablets believed to be annealed during ascent (see above), the samples here reflect OH contents that could only have been attained at pressures in excess of 3 GPa. These are minimum pressures because the OH contents are those calculated for $a_{H_2O} = 1$, i.e. water pressure equal to total pressure. Petrological studies of Monastery megacrysts are not compatible with their precipitation from pure water and suggest in contrast an incompatible-element-enriched silicate melt, with a_{H_2O} more probably in the range of 10^{-1} to 10^{-2} (see also discussion below). H_2O activities calculated from the olivine OH concentrations using the relationship established by Kohlstedt *et al.* (1996) are in this range (Table 3), but are somewhat higher than expected. At this stage the *a*–*X* relations of hydrous olivines at $P_{H_2O} < P_{total}$ remain to be established. In summary, however, the OH levels of these olivines were attained at substantial depths in the mantle, not necessarily different from their depths of origin. In particular, they are not compatible with resetting to crustal environments.

Correlations of OH with mineral composition

Concentrations of OH and other elements as a function of a differentiation index [Ca/(Ca + Mg) in clinopyroxenes, Mg-number in other phases] are plotted in Figs 5–8. All minerals show systematic variation in OH and other minor or trace element content with these indices, although the variation for OH in olivine is poorly defined as a result of a degree of sample heterogeneity. Chemical trends for many elements in these figures are characterized by two sections of different slope, corresponding to crystallization in the presence and absence of ilmenite, respectively (Gurney *et al.*, 1979). In the following section we discuss the trends for each mineral in turn.

Garnet

OH in garnet megacrysts for Monastery is positively correlated with Fe-enrichment as previously noted by Bell & Rossman (1992*b*) and illustrated in Fig. 5a. There is a change in slope in this correlation at Mg-number ~74, the H_2O enrichment trend flattening at more Fe-rich compositions. The change in slope of the H_2O–Mg-number trend corresponds to the point where ilmenite begins to crystallize from the parent magma (Gurney *et al.*, 1979), and appears in several other element trends with Mg-number (Fig. 5b–k). For some elements the trend flattens or reverses (Na_2O, TiO_2, V) whereas for others it steepens (Sc, Zr). The trends of the divalent transition metals (MnO, Ni) are not affected.

Clinopyroxene

OH in clinopyroxene is similar to garnet in displaying an initial enrichment, followed by change in slope associated

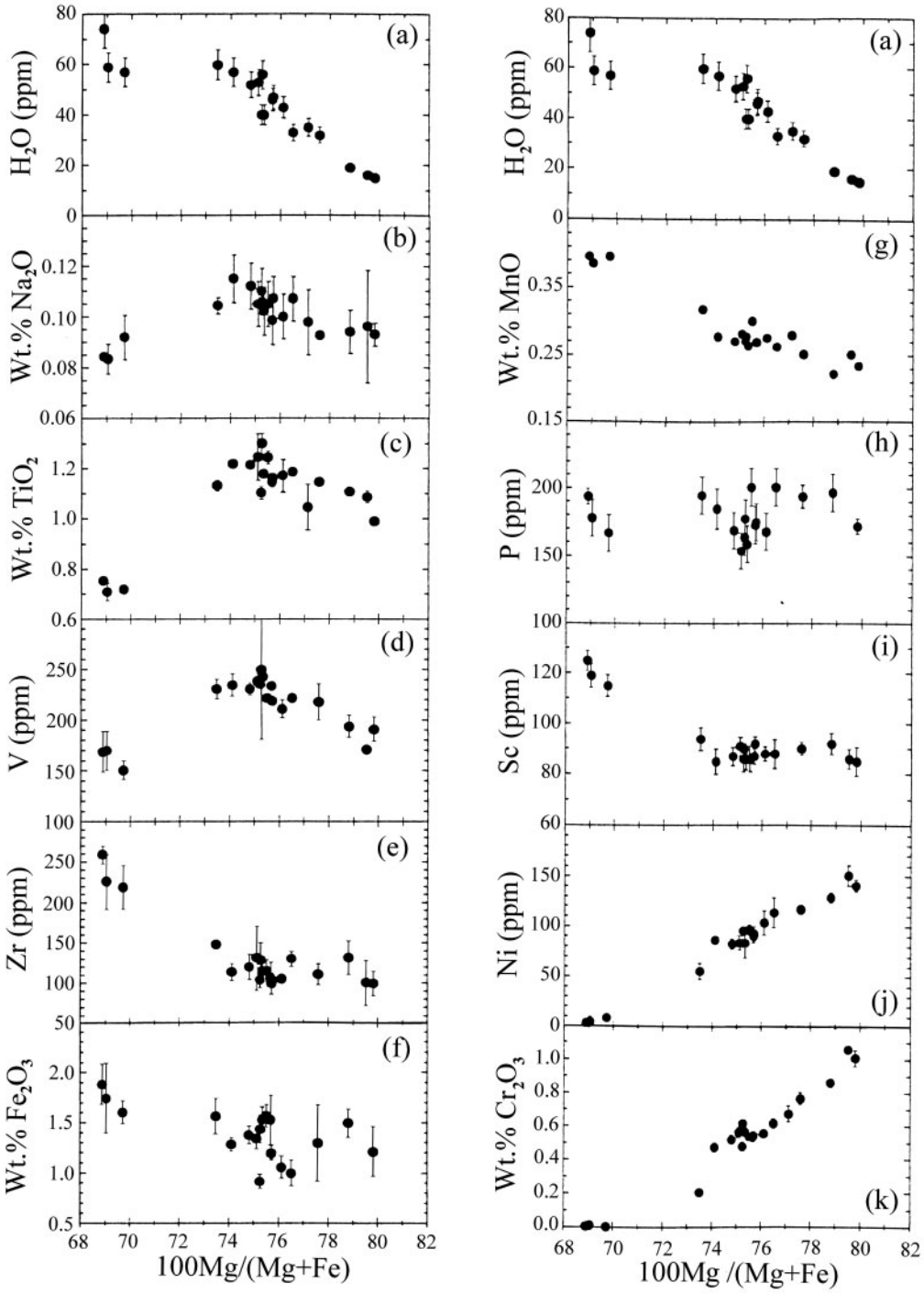

Fig. 5. Compositional trends of OH, expressed as ppm H_2O by weight (a), and other elements, determined by electron microprobe, (b–k) in Monastery garnet megacrysts as a function of Mg-number in the garnet. Part (a) is repeated above the second column of figures to facilitate comparison. Error bars represent 2σ calculated from repeat analyses (except for OH; see text), and reflect sample heterogeneity as well as counting statistics.

with ilmenite crystallization (Fig. 6a). One anomalous OH-rich clinopyroxene is present (MON26, a gt–cpx pair) in the initial ilmenite-free section of the trend, the remaining samples showing a slight positive correlation between OH and Ca-number. In contrast to garnet, the slope of the trend actually reverses and OH decreases in concentration in the ilmenite-present section of the trend. A similar trend is seen for K (Fig. 6e) and TiO_2 (Fig. 6b)

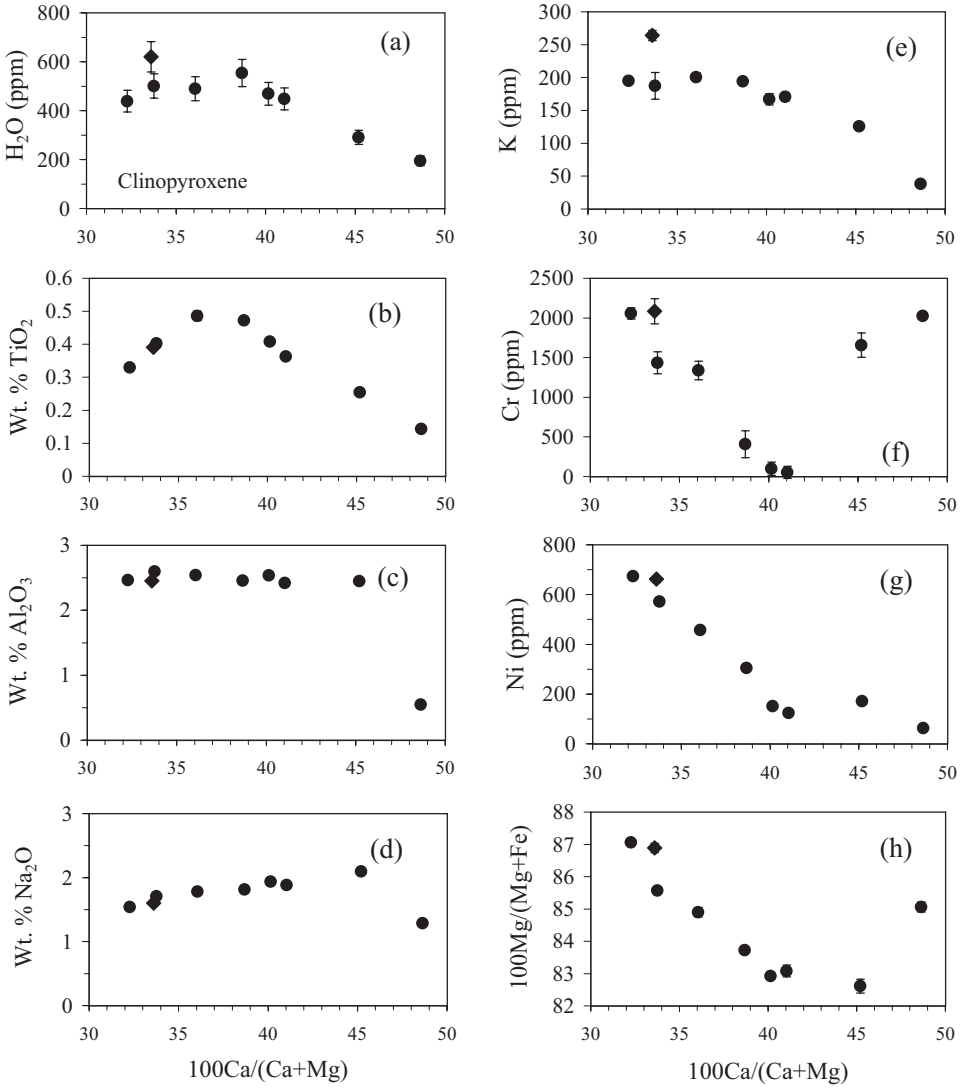

Fig. 6. OH expressed as ppm H_2O by weight (a) and other compositional variation (b–h) in clinopyroxene megacrysts from the Monastery kimberlite plotted as a function of Ca-number. Differentiation proceeds towards higher Ca-number [100Ca/(Ca + Mg)]. Error bars as for Fig. 5. The diamond symbol is clinopyroxene MON-26, from the garnet–cpx pair, and falls slightly off the trend established by the other samples for the elements H, K, Mg, Cr and Ni, but not for other elements (see text for discussion). Changes in slope of trends occur for H_2O, Ti, and K around ilmenite entry.

in clinopyroxene. In detail, it can be seen that OH occupies a position intermediate between these two elements. As in garnet, the divalent transition metals Mn (not shown) and Ni do not show a break in slope. The most calcic clinopyroxene, belonging to the low Zr/Nb group 3 association, has a very low OH content like some of the olivines of the low Zr/Nb group 2 suite.

Orthopyroxene

The three orthopyroxene samples show an apparent trend of decreasing OH with Fe-enrichment (Fig. 7a), although this trend is, strictly speaking, not outside the estimated experimental uncertainty. From the respective trends of minor element oxides and Ca-number with Mg-number (Fig. 7b, c and e), it is apparent that the orthopyroxene OH contents are not correlated with components affected by ilmenite crystallization, such as TiO_2, but are correlated with Al_2O_3, Ca-number and Na (not shown).

Olivine

For olivines of the low-Fe (MST) association, the scatter in OH data allows no clearly defined correlation with Fe-enrichment to be established (Figs. 3 and 8a), but is

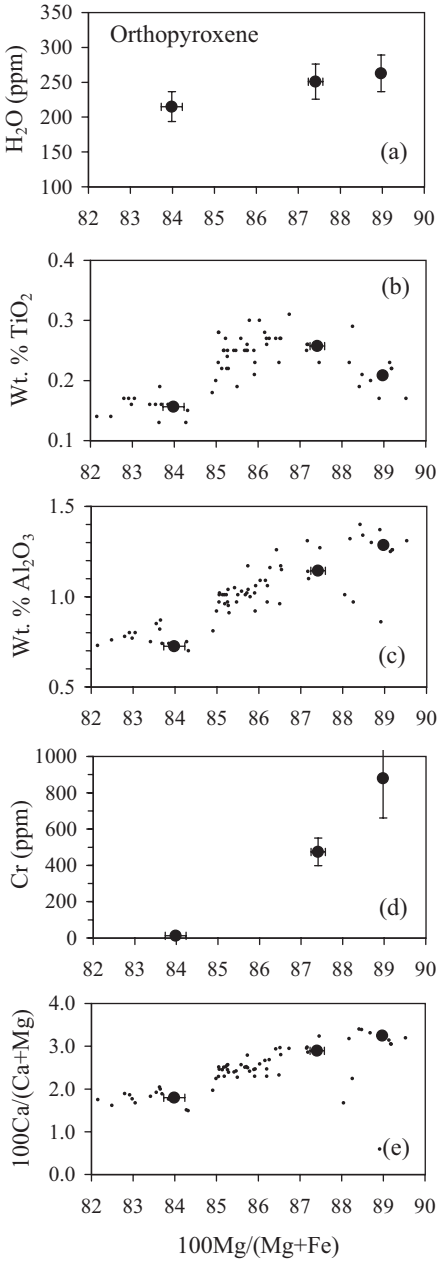

Fig. 7. OH expressed as ppm H_2O by weight, and selected minor element contents of orthopyroxene as a function of Mg-number. OH uncertainties are 10% relative (see text). Small dots in selected plots are Monastery orthopyroxene megacryst analyses from Moore (1986).

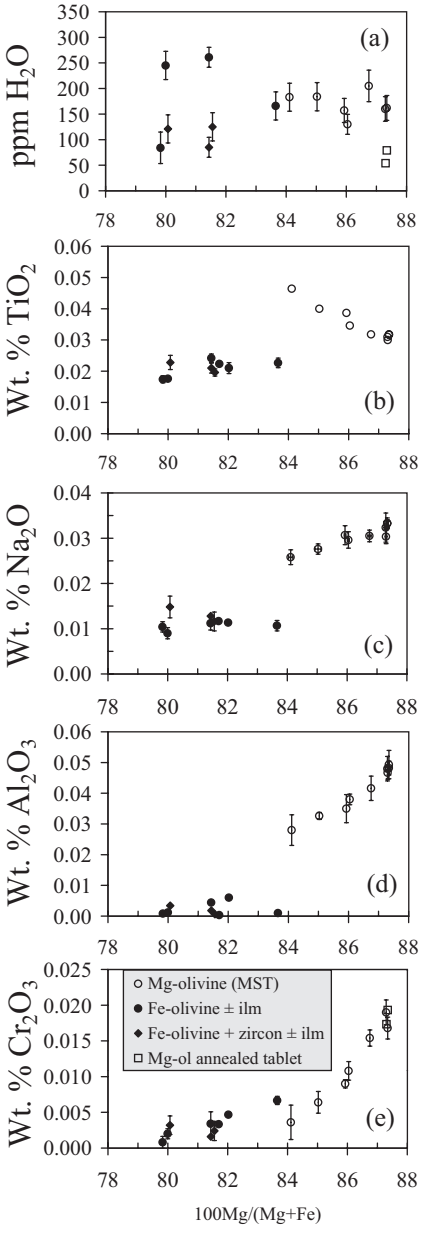

Fig. 8. Compositional trends of OH, expressed as ppm H_2O by weight, and other elements in olivine. In (a), the maximum observed OH content for each sample is plotted.

consistent with either no variation or a shallow positive correlation. Other trace elements show well-defined correlations with Mg-number in this group (Fig. 8b–e), supporting the consistent chemical evolution seen in clinopyroxene and garnet precipitated over the same temperature interval. The Fe-rich olivines contrast with this behavior and fall into two groups (Fig. 3). One group, which includes the three zircon–olivine intergrowths, shows a negative correlation between OH and Fe-enrichment, whereas the other group is represented by two samples with OH contents well above this trend. All the Fe-rich olivines are characterized by essentially constant trace element levels that are independent of Mg-number (Fig. 8b–e). With the exception of Ti, the trace element concentrations in these samples resemble those in low-temperature peridotites, whereas those in the MST olivines are similar to those in high-temperature peridotites (Hervig *et al.*, 1986).

ORIGIN OF OH CORRELATIONS

The above discussion serves to illustrate that, with the exception of certain olivine samples, the OH component in these megacrysts displays a coherent variation that is similar in its consistency and its inter-mineral variability to other minor and trace components. This suggests that, despite the high diffusivities of hydrous components in olivine, pyroxenes and garnet, these minerals preserve a signature that was established in their mantle source. The mantle origin of this OH is further confirmed by the high (subcrustal) pressures of water required by OH concentrations in olivine. In this section we explore in some detail the origin of these correlations.

Garnet

There are no correlations to suggest that H incorporation in this suite of garnets is governed by the stoichiometric charge balance requirements of other minor and trace element substitutions. The H abundances on an atomic basis are an order of magnitude lower than possible indices of charge imbalance, such as Ti + Zr + P − Na, which means that much more sensitive probes of garnet crystal chemistry (or more hydrous garnets) are required to evaluate conclusively the substitution mechanisms as far as minor elements are concerned.

The positive correlation of OH and Fe content for the garnet megacrysts is qualitatively consistent with progressive enrichment of incompatible elements in an evolving magma and its crystallization products (Bell & Rossman, 1992*b*). However, the initial OH enrichment for the ilmenite-free section of the garnet trend is from 15 to 57 ppm, or about a factor of four. This greatly exceeds the enrichment in Ti, for example, over the same interval. Petrological modeling (Bell *et al.*, 1995*a*) indicates that the degree of crystallization over this interval is in the range of 20–40%, implying an increase in melt H (or Ti) concentration by a factor of 1·25–1·55. If the petrological understanding of these samples is correct, then a threefold increase in the partitioning of OH between garnet and melt with Fe-enrichment is implied. At the very least there is a change in the distribution coefficient (D) for OH relative to those for other incompatible components over this interval of composition.

The flattening of the OH trend from the point of ilmenite entry is the opposite to what is expected for constant (or increasing) partitioning of OH between garnet and melt, because the co-crystallization of ilmenite will retard Fe-enrichment for a given degree of crystallization (Schulze, 1984). This should result in steepening of the trend, as observed for incompatible elements such as Zr (Fig. 5e) and Sc (Fig. 5i). The suppression of OH enrichment may result from changing (decreasing) D, or from the buffering effect of a hydrous phase entering the assemblage at this point. As discussed above, there is no hydrous mineral that crystallizes at this point (or at any stage in the evolution of the MST suite). However, the possibility of vapor phase saturation occurring at this point is worth some discussion and is examined below. In this section, the discussion is confined to possible causes of changing D, which, as implied above, involves first a progressive increase in D^{gt-liq}, followed by a decrease.

A partial explanation for the above behavior may be found in the apparent association between Ti and a certain component of the garnet OH, namely, that with OH absorption at 3512 cm^{-1} (Bell & Rossman, 1992*b*). Presumably, all OH sites in garnet increase proportional to an increase in water activity in the system, but the number of '3512 cm^{-1}' sites available progressively increases and then decreases as TiO_2 in the garnet changes (Fig. 5c). This results in accentuated build-up in OH over the initial interval where both Ti in garnet and melt water activity increase in response to differentiation, followed by a subdued increase at Mg-number <74, where the number of available OH sites associated with Ti decreases in response to the sudden reversal in Ti content of the garnet. This effect is nevertheless not sufficient to account for the apparent over-enrichment of OH during the initial stages of crystallization, because the proportion of 3512 cm^{-1} OH in the spectrum does not exceed about 50% (Fig. 2a).

The fact that H is enriched above the levels expected for simple proportional dependence on melt H content suggests a power-law dependence on the activity of melt H-species, e.g. $c_{OH} = k(a_{H_2O})^n$, where $n > 1$, and implies a reaction stoichiometry for OH incorporation with multiple H atoms per garnet formula unit. From the above discussion on Ti-associated OH sites it is apparent that the incorporation reactions are more complex than the simple hydrogarnet substitution (Flint *et al.*, 1941) and appear to involve melt activities of other components (such as Ti and Al). This, combined with the unknown dependence of a_{H_2O} on bulk H concentration in the melt, implies that quantitative extraction of a physically meaningful value of n is not possible at this stage (see also Poirier & Duba, 1997).

Clinopyroxene

The evolution of OH in clinopyroxene before ilmenite crystallization is consistent with constant or slightly decreasing partitioning of OH between clinopyroxene and its parent magma. The downturn in H_2O and K associated with the ilmenite-influenced downturn in TiO_2 at Ca-number >36 (Fig. 6) suggests an influence of Ti on the incorporation of these components into clinopyroxene. Gasparik (1985) has argued that Ti incorporation into synthetic kosmochlor ($NaCrSi_2O_6$ clinopyroxene) is accompanied by a vacancy, and Smyth *et al.* (1991) have shown a correlation between vacancy and

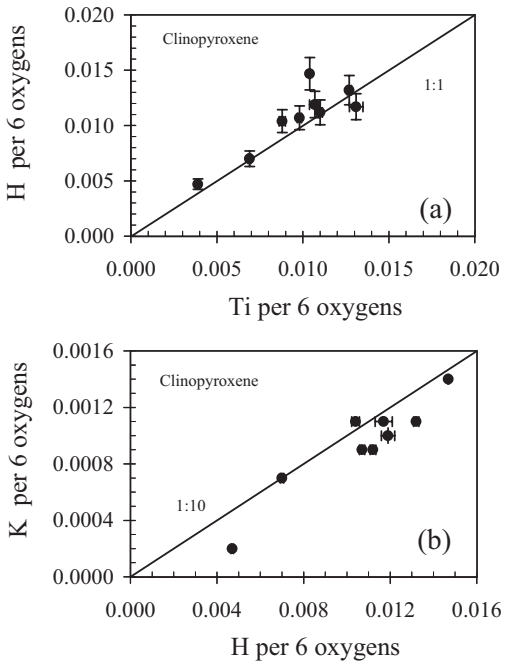

Fig. 9. Correlation of atomic H with (a) Ti and (b) K in clinopyroxene.

OH concentrations in omphacites. The approximately constant 1:1 ratio of Ti to H (Fig. 9a) in Monastery clinopyroxenes suggests a crystal-chemical association between the two. This association was, however, not found in other studies of natural clinopyroxenes (Skogby *et al.*, 1990; Smyth *et al.*, 1991) and may be coincidental in the present study. The fact that a similar behavior to OH is displayed by K, but at a factor of 10 lower atomic concentrations (Fig. 9b) indicates that this kind of trend can be produced without a specific 1:1 substitutional relationship.

It is not clear if the lower OH content of the calcic clinopyroxene reflects phlogopite co-crystallization, a different parent magma composition, different P–T conditions of origin, or aspects of the pyroxene crystal chemistry. All these factors may play a role in the OH content. Al and Fe^{3+} were identified by Skogby *et al.* (1990) as probable factors in OH incorporation into clinopyroxene. The progressive decrease in proportional abundance of the 3540 cm^{-1} band in the Monastery megacrysts suggests a change in proportion of OH associated with Fe (Skogby, 1994).

Sample MON26, which falls above the general OH–Ca-number trend for clinopyroxene is also enriched in K, Ni and Cr compared with the average trends for these elements. This sample may be the product of local interaction of the magma with phlogopite lherzolite wall-rock (the common mantle peridotite in the Monastery kimberlite) or a partial melt thereof. Such interaction in megacryst suites is suggested by occasional Sr or Nd isotopic heterogeneity in megacryst samples from any one suite (Jones, 1987; Hops *et al.*, 1992).

Orthopyroxene

The apparently continuous decline in orthopyroxene OH content with megacryst suite differentiation is opposite to that observed in garnet, and differs from what trends may be discerned from the clinopyroxene and olivine data in its monotonic quality. However, the positive correlation between Al and OH is consistent with experimental observations of Rauch & Keppler (2002) on the strong enhancing effect of Al upon OH incorporation in orthopyroxene. The megacryst orthopyroxenes also contain strong OH absorptions at high wavenumber of the type identified by Rauch & Keppler (2002) to result from OH associated with Al. The abundance variations and the spectral characteristics therefore both suggest a strong, and possibly dominant crystal chemical influence on OH incorporation in orthopyroxene.

Olivine

The data in Table 5 and Figure 8a–e indicate that there is no major or trace element determined in this study with which OH is consistently positively correlated in abundance for the entire sample suite. A large number of plots attempting to relate H to minor element substitutions or charge balance criteria were examined with no correlations observed (e.g. Fig. 10a and b). What was observed, however, were relatively strong correlations among the minor elements, excluding H; for example, the approximately 1:1 relationship between Na and Al + P (Fig. 10c) suggests a charge-coupled substitution. Similarly well-defined correlations (but not at 1:1) exist between other minor element combinations (e.g. Fig. 10d). It was generally observed that the addition of H to such plots disrupts the well-defined systematics. This suggests a negligible role of coupled trace element substitutions in controlling OH abundance for olivine. This result conflicts with the study of Kurosawa *et al.* (1997), who reported a correlation between total monovalent (including H^+) cations and trivalent cations (Al + Cr) in olivines from garnet peridotites. Our result is, however, in agreement with a number of experimental and theoretical studies of OH in olivine that predict substitution mechanisms for H involving the major olivine ions Fe, Mg, Si and O (Bai & Kohlstedt, 1992, 1993; Wright & Catlow, 1994; Kohlstedt *et al.*, 1996).

Because of the scatter in the OH data, the precise behavior of H during chemical evolution of the MST olivines cannot be determined. However, the overall lack of variation in comparison with the Fe-rich olivines, and the fact that a relatively consistent relationship is permitted by the error bars, suggests that abundances are close to those established during the magmatic stages of olivine history. However, the trend is indistinct

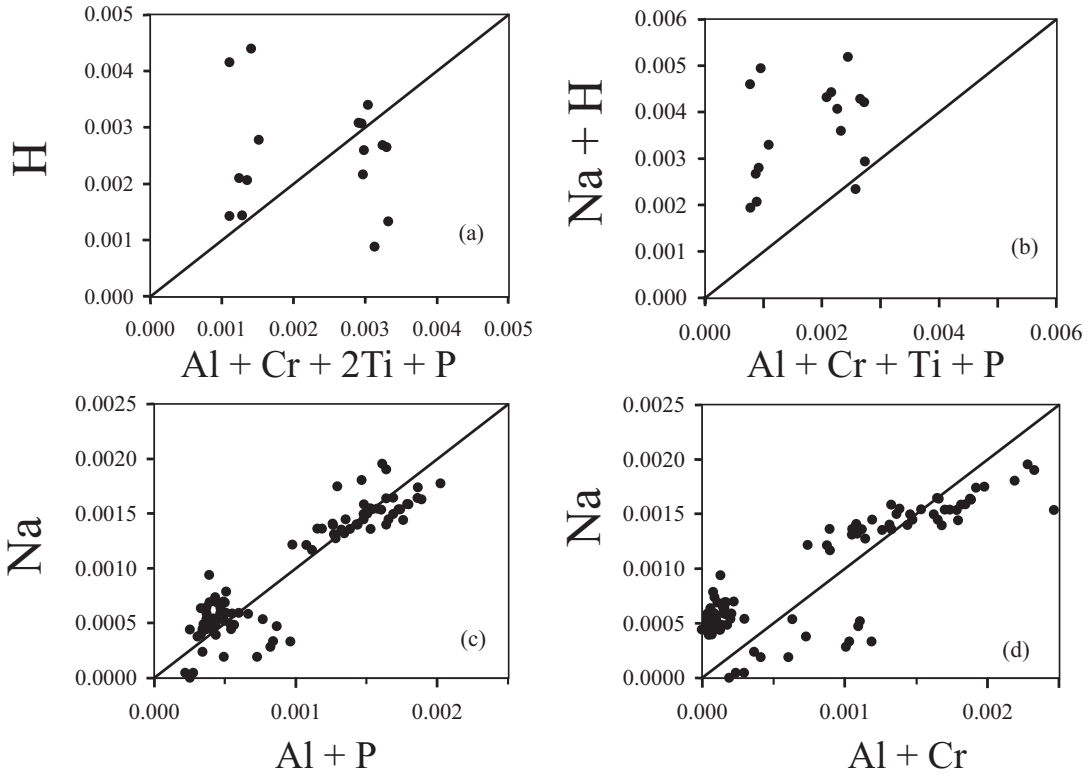

Fig. 10. H (atomic, per four oxygens) and minor elements in olivine: (a) H vs Al + Cr + 2Ti + P; (b) Na + H vs Al + Cr + Ti + P; (c) Na vs Al + P; (d) Na vs Al + Cr. In (a) and (b) the average concentrations are plotted for each sample. In (c) and (d), for which only electron microprobe data are used, individual analyses (3–5 per sample) are plotted, including four samples of olivine in garnet lherzolite from Lesotho and KBH-1, a spinel lherzolite from Kilbourne Hole.

because of the uncertainties regarding contributions from inclusions (e.g. molecular water), discussed above, as well as the possible effects of limited H loss or gain. The compositional evolution of these olivines in the absence of ilmenite is illustrated by the positive correlation between TiO_2 and Fe-enrichment (Fig. 8b). Other elements, such as Ca and Al, whose melt activities are effectively buffered by garnet and clinopyroxene are likely to be controlled in olivine by temperature-dependent partitioning (Agee & Walker, 1990; Köhler & Brey, 1990).

The origin among the high-Fe (group 2) olivines of both high-OH and low-OH olivines is problematic and further obscured by a poor understanding of the P–T–f_{H_2O} conditions of origin of this suite. The buffering effect of ilmenite on the TiO_2 contents of these olivines can be seen in Fig. 8b, contrasting with the well-defined trend of Ti enrichment for the Fe-poor olivines (that lack coexisting ilmenite). A similar explanation involving buffering of OH by phlogopite may explain the negative correlation of OH with Fe-enrichment in one group of Fe-rich olivines. It is also possible that the low-OH olivines have simply lost H and that the negative OH–Fe correlation in these samples reflects some internally buffered state.

Vapor phase saturation?

Although saturation in phlogopite or other hydrous minerals is believed not to be a factor in the evolution of MST suite megacrysts, it is possible that an H-rich fluid phase separates from the magma at the point where the trends in OH for garnet and clinopyroxene change slope. Evidence from experimental studies (Dalton & Presnall, 1998; Wyllie & Lee, 1999) of kimberlitic liquids in equilibrium with mantle minerals at these pressures suggests that with falling temperature the liquid retains or increases its CO_2 content, becoming carbonatitic, and precipitating a carbonate mineral at low temperatures, rather than saturating in CO_2. This suggests that a vapor phase that evolves in equilibrium with differentiating megacryst magma should be water rich. However, as the solubilities of water in silicate and carbonate melts in these conditions are of the order of tens of weight percent, the exsolution of a water-rich vapor implies very high concentrations of water in the melt. The water contents estimated for the megacryst magma from trace element systematics (see below) are considerably below expected saturation levels, even after 20–40% crystallization, and exsolution of a water-rich vapor is therefore considered unlikely.

Preservation of mantle signatures: a discussion

The coherent OH trends in garnet and clinopyroxene provide evidence that H has not been lost in a haphazard manner from these samples during eruption. This seems surprising in the light of high measured diffusivities for hydrous components in these minerals (Ingrin *et al.*, 1995; Wang *et al.*, 1996; Hercule & Ingrin, 1999; Carpenter *et al.*, 2000). Some disturbance in the case of olivine remains a possibility, but petrological factors in the source may also play a role. The coherent trends also argue against re-equilibration of the samples in a hydrous crustal environment, and it has been demonstrated that mantle water pressures are required for the OH levels in most olivines. One possible interpretation is that the H is completely decoupled (owing to grossly different diffusive timescales) from the silicate framework of the mineral and responds rapidly to external crustal conditions, whereas the silicate structural framework is essentially frozen, preserving a structure acquired in the mantle. In this case, the recorded H is some product of hydrogen fugacity in the kimberlite magma, or its immediate post-emplacement conditions, and the internally buffered metastable environment of the mineral structure, quenched from upper-mantle conditions. This type of dependence of OH incorporation on prior formation conditions has been demonstrated experimentally for olivine by Bai & Kohlstedt (1993) and for pyroxenes by Skogby (1994) and Guilhaumou *et al.* (1999).

Compositional trends of Monastery MST megacrysts for major and trace elements are remarkably regular and it may be expected that the environment for OH incorporation would be similarly coherent. However, it seems unlikely that an environment of kimberlite emplacement, cooling and hydrothermal alteration in a number of regimes could be so uniform that the imposed crustal H-species activity resulted in no disturbance of these mantle trends. It seems far more likely that the OH trends observed derive from mantle processes, and that the activity gradients required for H disturbance during ascent are not attained in kimberlite emplacement. Similar conclusions were drawn by Bell & Rossman (1992*b*) and Matsyuk *et al.* (1998) from detailed studies of garnets from diverse mantle environments.

Summary of OH correlations

For clinopyroxene and garnet, the relationship of OH to Mg-number (or Ca-number in cpx) is characterized by two sections of different slope, the change occurring where ilmenite becomes a co-crystallizing phase. For clinopyroxene and garnet this occurs during the magmatic evolution of a single petrological association, whereas for olivine, which also exhibits a more scattered relationship owing to later disturbance, it appears that two different petrological associations are involved. The initial positive correlation of OH with Fe-enrichment that occurs for the more Mg-rich samples is qualitatively what is expected for the evolution of a hydrous magma by crystallization of nominally anhydrous phases. However, the quantitative evaluation of these initial trends and the change (or reversal) in slope that occurs for the petrologically more evolved samples demonstrate that the controls on OH incorporation are not straightforward. The limited orthopyroxene data appear to confirm this inference, suggesting possible influence of Al on OH incorporation.

Two possible origins for the change in trend at the ilmenite-saturation point are considered. One is that minor element substitutions effected by ilmenite buffering change the partitioning behavior of OH. The other is that a hydrous phase begins to play a role in the magmatic evolution of the system at this point. There is at present no firm evidence for the latter, but the former possibility is supported by similar behavior to H for other trace elements, such as K and Na. We therefore interpret the regularly changing H_2O and minor element concentrations, illustrated in Figs 5–8, to reflect changing elemental concentrations in the evolving melt phase *and* the variation in response to temperature, mineral chemistry and melt chemistry of mineral–melt distribution coefficients.

INTER-MINERAL PARTITIONING OF OH

Ideally, the study of inter-mineral partitioning should proceed by analysis of spatially adjacent mineral grains, a procedure that is difficult in megacryst suites because coexisting intergrown megacrysts are relatively uncommon. However, the systematic relationships between composition (both major and trace elements) and degree of chemical differentiation for each mineral species are such that equilibrium partitioning relationships between mineral species are readily established by interpolation between analyses of occasional coexisting pairs (e.g. Gurney *et al.*, 1979). We use this principle to calculate inter-mineral partition coefficients for OH. The validity of this procedure is confirmed by measurements of OH partition coefficients in the few samples where physically coexisting pairs are available for analysis and, in general, for other elements where more data on coexisting pairs are available (Moore, 1986; Bell *et al.*, 1995*c*).

Coexisting compositional relationships described in the literature, supplemented by data reported here, were parameterized by a series of linear or second-order polynomial equations (Table A1, Appendix). For any given megacryst mineral, these equations allow calculation of the major element compositions (either Mg-number or

Ca-number) of the other minerals with which it is in equilibrium. The H_2O contents of these minerals can then be calculated from the H_2O–Mg-number trends established by individual mineral analysis using regression equations derived from the data in Figs 5a, 6a, 7a and 8a (Table A1, Appendix). The inter-mineral distribution coefficients were thus calculated from the measured OH content of a given mineral sample and the calculated OH content of the phases with which it is predicted to be in equilibrium.

Partitioning relationships involving garnet

The calculated distributions of OH between garnet and clinopyroxene, orthopyroxene and olivine as a function of garnet Mg-number are shown in Fig. 11a–c, respectively, together with the measurements of OH partitioning in coexisting garnet–clinopyroxene (MON26) and garnet–olivine (MON24) pairs. The agreement between the *D* values calculated from the garnet data and those from the clinopyroxene data is a reflection of the well-defined trends that H_2O follows with Mg-number and Ca-number in these minerals, respectively. Despite the fact that the trend of OH incorporation into both garnet and clinopyroxene changes slope at the point of ilmenite entry (Figs 5a and 6a), the distribution of OH between these phases displays a monotonic variation, with no change in the trend of inter-mineral partitioning. The calculations for olivine are not as precise as for the other phases because olivine is substantially more heterogeneous with respect to OH than the other minerals. In the case of olivine we have assumed, based on observations discussed above, that the most OH-rich measurement represents the closest approach to the equilibrium mantle value.

It is immediately obvious from Fig. 11 that partitioning of OH between garnet and other phases is not constant. However, all three minerals display a similar sense of variation in their partitioning of OH with garnet. The first-crystallized clinopyroxene incorporates about 50 times more OH than its coexisting garnet, diminishing to a factor of about 5× for the clinopyroxenes coexisting with the most Fe-rich garnets. $D_{H_2O}^{opx-gt}$ varies from 18 at high Mg-number to ~4 at low Mg-number, where the minerals coexist with ilmenite. Olivine and garnet coexist over a more restricted range of the differentiation sequence than garnet, clinopyroxene and orthopyroxene, but the overall variation in $D_{H_2O}^{ol-gt}$ (from ~14 to ~3) is similar to that of $D_{H_2O}^{opx-gt}$, about half the relative change in $D_{H_2O}^{cpx-gt}$.

Much of the change in inter-mineral D_{H_2O} involving garnet occurs over the first 50–80°C of the megacryst evolution and is related to very low OH content of garnet under these conditions. Possible crystal chemical reasons for rapidly changing OH in garnet have been discussed above, but temperature is an additional factor that may influence OH incorporation. For example, Lu & Keppler (1997) observed that OH content of Dora Maira pyrope decreased with rising temperature under hydrothermal upper-mantle conditions.

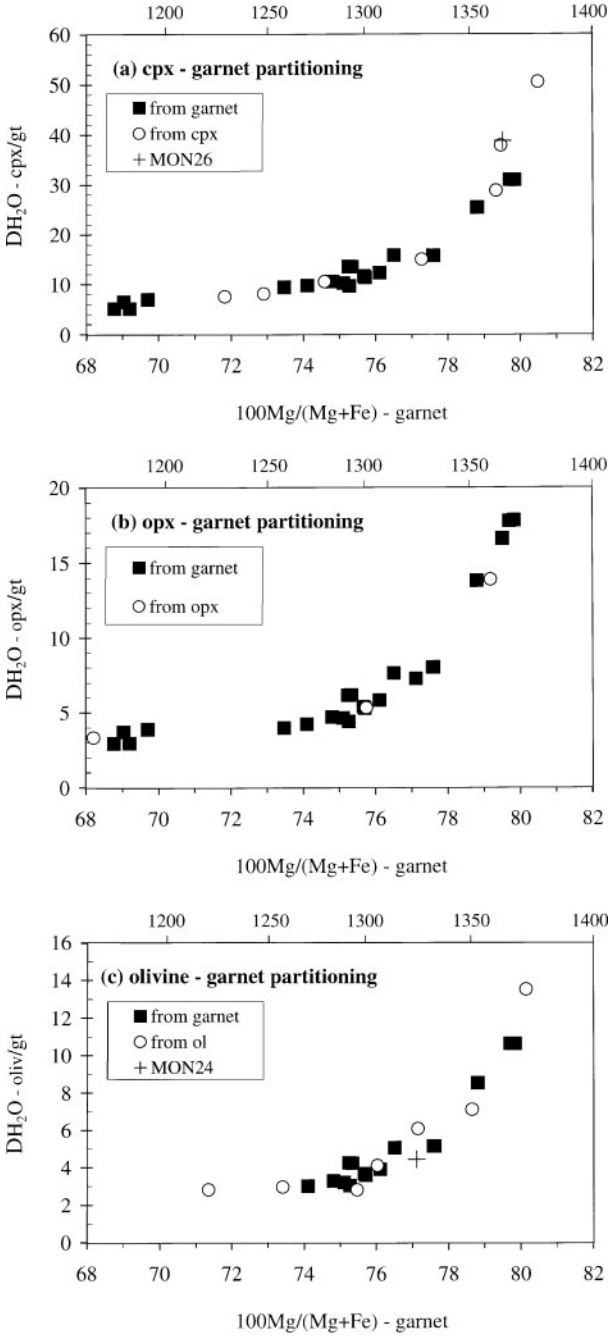

Fig. 11. Partitioning of OH (expressed as H_2O) between garnet and (a) clinopyroxene, (b) orthopyroxene and (c) olivine, as a function of Mg-number in garnet, with corresponding temperatures indicated (see text and caption to Fig. 12). Distribution coefficients are calculated as described in the text, and measured in the case of the two coexisting pairs, MON-24 (gt–ol) and MON-26 (gt–cpx).

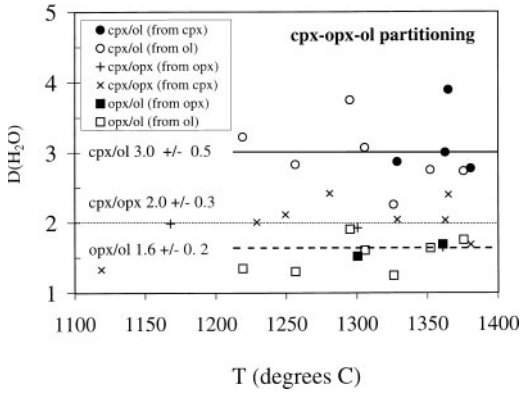

Fig. 12. Partitioning of OH (expressed as H_2O) between clinopyroxene/olivine, clinopyroxene/orthopyroxene and orthopyroxene/olivine as a function of temperature. Temperatures are the averages of the methods of Taylor (1998) and Brey & Köhler (1990), both computed at 5·0 GPa. Distribution coefficients were calculated as described in the text. The horizontal lines are the mean D_{H_2O} values for the three sets of mineral pairs, illustrated by circles, crosses and squares, respectively.

Olivine–orthopyroxene–clinopyroxene partitioning

In contrast to partitioning relationships involving garnet, the distribution of OH between olivine, clinopyroxene and orthopyroxene is relatively uniform. This is shown in Fig. 12, where the calculated D_{H_2O} values for cpx/ol, cpx/opx and opx/ol are plotted as a function of temperature. The temperatures are monotonically related to Ca-number in clinopyroxene and are calculated from synthetic coexisting mineral compositions interpolated from the natural dataset of coexisting phases. As a result of the uncertainties in accuracy of various thermometers, and the fertile compositions of the megacrysts, the average of two modern calibrations (Brey & Köhler, 1990; Taylor, 1998) is used in these figures. In all three cases, the D_{H_2O} values are more or less consistent with a single distribution coefficient for each mineral pair, independent of mineral composition and temperature over the range investigated. This is a noteworthy point, considering the variation in the OH abundances of the individual minerals and the changes in slope exhibited by their OH trends. The partitioning of OH between ortho- and clinopyroxene in megacrysts [$D_{H_2O}^{cpx/opx} = 2{\cdot}0 \pm 0{\cdot}3(1\sigma, n = 11)$] is coincident with the range of values of Peslier *et al.* (2002) [$D_{H_2O}^{cpx/opx} = 2{\cdot}2 \pm 0{\cdot}5(1\sigma, n = 17)$] and those derived from the data of Bell & Rossman (1992*b*) for peridotites and a garnet websterite [$D_{H_2O}^{cpx/opx} = 2{\cdot}6 \pm 0{\cdot}4(1\sigma, n = 5)$]. These latter values are, however, somewhat less accurately determined because of the analytical method employed in that study (unpolarized spectra in some cases). In contrast, partitioning of OH between olivine and the pyroxenes is grossly different. $D_{H_2O}^{px/ol}$ is far higher in the study by Bell & Rossman (1992*b*) because of the very low OH concentrations in olivines from basalt-hosted spinel lherzolite xenoliths. That study also employed a different calibration for the OH content of olivine, which resulted in concentration estimates 0·7 times lower than would be derived from the calibration used here.

Olivine–zircon partitioning

The three olivine–zircon intergrowths yield a mean $D_{H_2O}^{ol-zir} = 3{\cdot}2 \pm 0{\cdot}9(2\sigma, n = 4)$, assuming that the heterogeneities seen in both olivine and zircon in ROM181 are correlated. These samples represent a more chemically evolved system than the other samples, and this partition coefficient is likely to represent temperatures, and possibly pressures, lower than those of the other megacrysts.

PARTITIONING OF OH BETWEEN MINERALS AND MELT

Absolute values of $D_{H_2O}^{mineral-melt}$ are difficult to infer because of uncertainties in parent magma H_2O content. It is often proposed that megacryst magmas are the precursor magmas to kimberlites. However, direct analysis of the H_2O content of kimberlite rocks is inappropriate, because they have exchanged with and been altered by hydrothermal fluids (Sheppard & Dawson 1975), in addition to being subject to degassing processes. An alternative approach is provided by the observation that water in undegassed mantle-derived magmas exhibits systematic concentration variations in relation to other trace elements (Dixon *et al.*, 1988; Michael, 1988, 1995; Danyushevsky *et al.*, 2000). The megacryst parent magmas derive from mildly depleted source regions that are geochemically very similar to ocean island basalt (OIB) sources and, unlike the erupted kimberlite, show minimal effects of interaction with enriched continental lithosphere (Jones, 1987; Nowell *et al.*, 1999).

We have used the correlations of H_2O with Ce, K_2O and P_2O_5 in oceanic basalts to provide three independent estimates of the H_2O content of the melt parental to the Monastery megacrysts. The water content was derived by extrapolating the trends in Ce/H_2O vs Ce, K_2O/H_2O vs K_2O and P_2O_5/H_2O vs P_2O_5 observed for a large literature database of mid-ocean ridge basalt (MORB) and OIB to the abundances of Ce, K_2O and P_2O_5 in the megacryst magma. The abundances of Ce, K_2O and P_2O_5 in the megacryst magma derive from analyses of the Monastery kimberlite, corrected for the petrographically observed assimilation of lithospheric mantle. These methods give estimates of $4{\cdot}2^{+1{\cdot}1}_{-1{\cdot}9}$, $2{\cdot}3^{+2{\cdot}3}_{-1{\cdot}0}$, and $1{\cdot}8^{+1{\cdot}1}_{-0{\cdot}4}$ respectively, with a mean of 2·8 ± 1 wt % H_2O. The error estimates represent approximately 95% confidence levels. Sources of error include scatter within the basalt data arrays and uncertainties in the extrapolations from the basalt data to the higher incompatible element concentrations observed in kimberlite-like melts. Given the

Table 6: Partition coefficients for H_2O

	D_{H_2O}	
	This study	Other studies
Inter-mineral		
cpx/opx	2·0 ± 0·3	2·6 ± 0·35[1]; 2·2 ± 0·5[2]
opx/olivine	1·6 ± 0·2	
cpx/olivine	3·0 ± 0·5	
olivine/zircon	3·4 ± 0·3	
cpx/garnet	5–50	
opx/garnet	4–18	
olivine/garnet	3·5–14	
Mineral–melt		
olivine/melt	0·0053–0·0046	0·040 ± 015 (1·5 GPa)[3]; 0·13 ± 03 (6 GPa)[3]
		0·002–0·005[4]
opx/melt	0·0093–0·0059	0·0035 ± 005 (<0·1 GPa)[5]
cpx/melt	0·016–0·013	
garnet/melt	0·0003–0·0014	
Rock–melt		
gt. lherz/melt	0·0063–0·0051	
sp. lherz/melt		~0·015[6]

Column 1: inter-mineral partition coefficients as shown in Figs 11 and 12. Mineral–melt calculated from measured OH in minerals and initial melt H_2O content of 2·8 ± 1·0 wt % as deduced from trace element systematics (see text). The range reported is that appropriate to conditions of megacryst fractionation from 1400°C to 1250°C (range reported from high to low temperature), and is derived by dividing the measured mineral H_2O contents by the calculated value in the corresponding melt, starting at 2·8 wt % and assuming that melt evolution proceeds by fractionation of the observed megacryst minerals in proportion $ol_{55}opx_{15}cpx_{15}gt_{15}$. It should be noted that this is only a portion of the compositional range used to describe inter-mineral partitioning. The values reported are uncertain to ~ ±40%, the error dominated by uncertainty in parental melt H_2O content. The garnet lherzolite/melt partition coefficient is calculated from the above data assuming primitive mantle mineral proportions (McDonough, 1990). Column 2 data studies: [1]Bell & Rossman (1992*a*); [2]Peslier *et al*. (2002); [3]Sweeney *et al*. (1997); [4]calculated from independent experiments on the solubility of water in olivine and silicate melts (see text); [5]Dobson *et al*. (1995); [6]Dixon *et al*. (1988) and Sims & De Paolo (1997).

higher pressure of megacryst and kimberlite genesis, the K and P derived estimates may be more reliable because both these elements, like H, show evidence for enhanced incorporation into mantle minerals at high pressures (Bishop *et al.*, 1978; Edgar & Vukadinovic, 1993; Kohlstedt *et al.*, 1996; Harlow, 1997). In contrast, Ce shows some evidence for a decrease (Sims & De Paolo, 1997).

The calculated range of D values is compared with other estimates in Table 6. Values for $D_{opx-melt}$ are comparable with, but slightly lower than those deduced by Dobson *et al.* (1995) for orthopyroxenes in a boninitic glass. $D_{ol-melt}$ values are approximately an order of magnitude lower than those estimated by Sweeney *et al.* (1997), who used elastic recoil detection analysis (ERDA) to analyze H in their experimental run products. That study, however, is not consistent with previous experimental work, in that inferred water contents of the olivines in the water-undersaturated melts exceed by up to a factor of 10 the saturation values measured for olivine in equilibrium with pure water (Kohlstedt *et al.*, 1996). Closer agreement is evident between our study and olivine–melt D_{H_2O} of 0·002–0·005, calculated by combining the results of Kohlstedt *et al.* (1996) with broad estimates of H_2O solubility in silicate melt at 5 GPa (~30–40 wt %).

The bulk D_{H_2O} for peridotite–melt, calculated by combining the individual mineral D values with their modal proportions, is ~0·005–0·006. This is similar to the value of ~0·01 inferred for basalt generation (Dixon *et al.*, 1988; Michael, 1988; Danyeshevsky *et al.*, 2000). In considering the melting of heterogeneous mantle, the presence of garnet pyroxenite bodies within peridotite is predicted to have a relatively minor effect on bulk D_{H_2O} because calculated D_{H_2O} for a 50–50 garnet–clinopyroxene mixture under the conditions examined here is ~0·008.

IMPLICATIONS FOR PLANETARY EVOLUTION

This study confirms previous results that pyroxenes and olivine are significant hosts for water in the upper mantle. Relative mineral abundances combined with the observed partitioning suggest that olivine is the dominant reservoir of H (~40%) in garnet peridotite at 5 GPa, with enstatite and diopside each containing about 30% of the total H. Garnet hosts less than 1%.

OH is strongly partitioned into the liquid phase during high P–T igneous processes in planetary interiors. However, from the results presented here and previous studies of basalts genesis, a consistent picture is emerging that this solid-incompatibility is only moderate. Water may therefore not be removed as readily from the Earth's interior as some other volatiles (e.g. Cl and some noble gases). The very high ratio of surface to interior hydrogen in the Earth, which is similar to the distribution of elements with much higher incompatibility, such as Cl, Ba or U, indicates that partial melting of the mantle, as observed today, is not responsible for maintaining this distribution of H. More extreme partitioning is required, such as that expected in fluid-mediated processes of H transfer in subduction zones.

The increasing solubility of H in olivine as a function of pressure (Kohlstedt *et al.*, 1996) and its higher measured concentrations in deep natural samples, such as these

megacrysts, suggests that H compatibility increases with depth. The reported decline in OH content of garnet at high pressure (Withers *et al.*, 1998) does not affect this tendency because of the low relative contribution of garnet to the overall OH budget of the mantle. Together with the lower extents of adiabatic partial melting at depth, the increasing H compatibility in mantle assemblages implies that the efficiency of H extraction by melting decreases with depth in the upper mantle. Pressure-dependent partitioning of H therefore acts to restrict degassing of H_2O to the shallowest part of the mantle. In addition to retarding H transfer to the exosphere, this will also reduce the tendency of high-pressure, low fraction melts to strengthen the mantle through H removal, as may occur at shallower levels (Karato, 1986; Hirth & Kohlstedt, 1996).

Moderate compatibility of H_2O during melting also implies that geophysically significant concentrations ($\sim$100–200 ppm, approximately those of the MORB source) may be retained in mantle residues during hydrous melting of the mantle above subduction zones. The predicted weakening effect of this H suggests easier remixing of such mantle compared with dehydrated oceanic lithosphere, and therefore a possible means to disperse modest quantities of recycled water into the upper mantle.

SUMMARY AND CONCLUSIONS

Cogenetic megacryst minerals from the Monastery kimberlite display correlated variations in OH, major and minor element composition which reflect bulk chemical evolution as a result of igneous differentiation as well as the effects of temperature and composition on interphase partition coefficients. During this evolution, water concentration in the parent magma is expected to increase monotonically, there being no independent evidence for vapor saturation. In the initial stages, dominated by silicate crystallization, OH contents of garnet and clinopyroxene appear to reflect this increase. H in garnet increases more rapidly (by a factor of 3–4) than the inferred melt H build-up. In later stages, where ilmenite crystallization is significant, the partitioning of H between melt and minerals is changed, apparently by a crystal chemical effect of Ti on the ability of garnet and clinopyroxene to incorporate H, although inter-mineral H partitioning changes smoothly through this transition. In clinopyroxene, a very similar pattern of compositional evolution to that of OH is seen for K.

From experimental evidence, the OH contents of megacryst garnets and olivines are consistent with their petrogenetic history in the mantle as crystallization products of a water-bearing melt at $\sim$50 kbar pressure, although some olivines with recrystallized textures appear to have equilibrated with lower water fugacities as they annealed during or after transport from the mantle. The regular behavior and consistent partitioning systematics observed throughout the suite for OH and all other elements suggests that H contents of garnet and pyroxenes are not generally disturbed from original mantle values. More scattered trends in olivine may result from hydrous inclusions and/or partial H loss in some grains or portions of grains.

Calculated and measured partitioning of OH between coexisting minerals is either invariant (cpx/ol = 3·0 ± 0·5; cpx/opx = 2·0 ± 0·3; opx/ol = 1·6 ± 0·2) or a smooth function of composition and temperature (1380–1150°C) for partitioning involving garnet. The inter-mineral partitioning relationships indicate that although higher OH concentrations may be found in modally less important clinopyroxene, just under half the water in nominally anhydrous mantle peridotite is contained in olivine, which may therefore represent the dominant mineral reservoir of water in the Earth's upper mantle and in other rocky planetary interiors.

The calculated distribution coefficients for water between these minerals and their parent magma ($D_{H_2O}^{cpx-melt} = 0{\cdot}013$–$0{\cdot}016$; $D_{H_2O}^{opx-melt} = 0{\cdot}006$–$0{\cdot}009$; $D_{H_2O}^{ol-melt} = 0{\cdot}0046$–$0{\cdot}0053$; $D_{H_2O}^{gt-melt} = 0{\cdot}0003$–$0{\cdot}0014$; $D_{H_2O}^{gtlhz-m} = 0{\cdot}0051$–$0{\cdot}0063$, all values ±40% uncertain) are broadly consistent with bulk partitioning relationships established for water from petrogenetic studies on MORB, and from laboratory measurements of H solubility in minerals and melts. A consistent picture for the partitioning behavior of H in the principal minerals of the upper mantle is emerging.

ACKNOWLEDGEMENTS

This paper has benefited from discussions with J. E. Dixon, P. D. Ihinger and E. M. Stolper, helpful reviews by J. Dixon and H. Keppler, and the perceptive comments of an anonymous reviewer. We thank Mr S. Gasson of Winburg, South Africa, for permission to visit and sample the Monastery kimberlite, and J. J. Gurney and A. P. le Roex (University of Cape Town) for supporting supplementary studies on the Monastery megacrysts. We acknowledge the assistance and expertise of J. T. Armstrong (Caltech) and C. Hadidiacos (Geophysical Laboratory) in electron probe trace microanalysis. This research was supported by NSF grants EAR 88-16006, EAR 91-040459 and EAR 92-18980 to G.R.R. D.R.B. acknowledges support from the DOE Office of Basic Energy Sciences (DE-FG02-93ER14400) and the Geophysical Laboratory, Carnegie Institution of Washington.

REFERENCES

Agee, C. B. & Walker, D. A. (1990). Aluminum partitioning between olivine and ultrabasic silicate liquid to 6 GPa. *Contributions to Mineralogy and Petrology* **105**, 243–254.

Armstrong, J. T. (1988). Quantitative analysis of silicate and oxide materials: comparison of Monte Carlo, ZAF and $\phi(\rho z)$ procedures. In: Newbury, D. E. (ed.) *Microbeam Analysis 1988*. San Francisco, CA: San Francisco Press, pp. 239–246.

Armstrong, J. T. (1991). Quantitative elemental analysis of individual microparticles with electron beam instruments. In: Heinrich, K. F. J. & Newbury, D. E. (eds) *Electron Probe Quantitation*. New York: Plenum, pp. 261–316.

Arredondo, E. H., Rossman, G. R. & Lumpkin, G. R. (2001). Hydrogen in spessartine–almandine garnets as a tracer of granitic pegmatite evolution. *American Mineralogist* **86**, 485–490.

Bai, Q. & Kohlstedt, D. L. (1992). Substantial hydrogen solubility in olivine and implications for water storage in the mantle. *Nature* **357**, 672–674.

Bai, Q. & Kohlstedt, D. L. (1993). Effects of chemical environment on the solubility and incorporation mechanism for hydrogen in olivine. *Physics and Chemistry of Minerals* **19**, 460–471.

Bell, D. R. & Ihinger, P. D. (2000). The isotopic composition of hydrogen in nominally anhydrous mantle minerals. *Geochimica et Cosmochimica Acta* **64**, 2109–2118.

Bell, D. R. & Mattioli, G. S. (1994). Oxidation state of iron in upper mantle garnets. *EOS Transactions, American Geophysical Union* **75**, 605.

Bell, D. R. & Rossman, G. R. (1992*a*). Water in Earth's mantle; the role of nominally anhydrous minerals. *Science* **255**, 1391–1397.

Bell, D. R. & Rossman, G. R. (1992*b*). The distribution of hydroxyl in garnets from the sub-continental mantle of southern Africa. *Contributions to Mineralogy and Petrology* **111**, 161–178.

Bell, D. R., Gurney, J. J., Le Roex, A. P., Moore, R. O. & Shimizu, N. (1995*a*). Compositional evolution of the Monastery megacrysts and parent magma. *Extended Abstracts, 6th International Kimberlite Conference*. Novosibirsk: Siberian Branch, Russian Academy of Sciences, pp. 50–51.

Bell, D. R., Ihinger, P. D. & Rossman, G. R. (1995*b*). Quantitative analysis of OH in garnet and pyroxenes. *American Mineralogist* **80**, 465–474.

Bell, D. R., Schulze, D. J., Read, G. H., Mattioli, G. S., Shimizu, N., Moore, R. O. & Gurney, J. J. (1995*c*). Geochemistry of Cr-poor megacrysts from the Lace (Group II) kimberlite, South Africa. *Extended Abstracts, 6th International Kimberlite Conference*. Novosibirsk: Siberian Branch, Russian Academy of Sciences, pp. 52–53.

Bell, D. R., Rossman, G. R., Maldener, J., Endisch, D. & Rauch, F. (2003). Hydroxide in olivine: a quantitative determination of the absolute amount and calibration of the IR spectrum. *Journal of Geophysical Research* **108**(B2), 2105, doi:10.1029/2001JB000679.

Beran, A., Langer, K. & Andrut, M. (1993). Single crystal infrared spectra in the range of OH fundamentals of paragenetic garnet, omphacite and kyanite in an eclogitic mantle xenolith. *Mineralogy and Petrology* **48**, 257–268.

Bishop, F. C., Smith, J. V. & Dawson, J. B. (1978). Na, K, P and Ti in garnet, pyroxene and olivine from peridotite and eclogite xenoliths from African kimberlites. *Lithos* **11**, 155–173.

Boullier, A.-M. & Nicolas, A. (1973). Texture and fabric of peridotite nodules from kimberlite. In: Nixon, P. H. (ed.) *Lesotho Kimberlites*. Maseru: Lesotho National Development Corporation, pp. 57–66.

Boullier, A.-M. & Nicolas, A. (1975). Classification of textures and fabrics of peridotite xenoliths from South African kimberlites. *Physics and Chemistry of the Earth* **9**, 467–476.

Boyd, F. R. & Nixon, P. H. (1973). Origin of the ilmenite–silicate nodules in kimberlites from Lesotho and South Africa. In: Nixon, P. H. (ed.) *Lesotho Kimberlites*. Maseru: Lesotho National Development Corporation, pp. 254–268.

Brey, G. P. & Köhler, T. (1990). Geothermobarometry in four phase lherzolites II. New thermobarometers and practical assessment of existing thermobarometers. *Journal of Petrology* **31**, 1353–1378.

Carpenter, S. J., Mackwell, S. J. & Dyar, M. D. (2000). Hydrogen in diopside diffusion profiles. *American Mineralogist* **85**, 480–488.

Dalton, J. A. & Presnall, D. C. (1998). The continuum of primary carbonatitic–kimberlitic melt compositions in equilibrium with lherzolite. Data from the system $CaO–MgO–Al_2O_3–SiO_2–CO_2$ at 6 GPa. *Journal of Petrology* **39**, 1953–1964.

Danyushevsky, L. V., Eggins, S. M., Falloon, T. J. & Christie, D. M. (2000). H_2O abundance in depleted to moderately enriched mid-ocean ridge magmas; Part 1: Incompatible behaviour, implications for mantle storage, and origin of regional variations. *Journal of Petrology* **41**, 1329–1364.

Davies, G. R., Spriggs, A. J. & Nixon, P. H. (2000). A non-cognate origin for the Gibeon kimberlite megacryst suite, Namibia: implications for the origin of Namibian kimberlites. *Journal of Petrology* **42**, 159–172.

Dawson, J. B., Hervig, R. L. & Smith, J. V. (1981). Fertile iron-rich dunite xenoliths from the Bultfontein kimberlite, South Africa. *Fortschritte der Mineralogie* **59**, 303–324.

Dixon, J. E., Stolper, E. M. & Delaney, J. R. (1988). Infrared spectroscopic measurements of CO_2 and H_2O in Juan de Fuca Ridge basaltic glasses. *Earth and Planetary Science Letters* **90**, 87–104.

Dobson, P. F., Skogby, H. S. & Rossman, G. R. (1995). Water in boninite glass and coexisting orthopyroxene: concentration and partitioning. *Contributions to Mineralogy and Petrology* **118**, 414–419.

Drury, M. R. & Van Roermund, H. L. M. (1988). Metasomatic origin for Fe–Ti-rich multiphase inclusions in olivine from kimberlite xenoliths. *Geology* **16**, 1035–1038.

Drury, M. R. & Van Roermund, H. L. M. (1989). Fluid assisted recrystallisation in upper mantle peridotites from kimberlites. *Journal of Petrology* **30**, 133–152.

Edgar, A. D. & Vukadinovic, D. (1993). Potassium-rich clinopyroxene in the mantle: an experimental investigation of a K-rich lamproite up to 60 kbar. *Geochimica et Cosmochimica Acta* **57**, 5063–5072.

Eggler, D. H., McCallum, M. E. & Smith, C. B. (1979). Megacryst assemblages in kimberlite from northern Colorado and southern Wyoming: petrology, geothermometry–barometry and areal distribution. In: Boyd, F. R. & Meyer, H. O. A. (eds) *The Mantle Sample: Inclusions in Kimberlites and Other Volcanics*. Washington, DC: American Geophysical Union, pp. 213–226.

Flint, E. P., McMurdie, H. F. & Wells, L. S. (1941). Hydrothermal and X-ray studies of the garnet–hydrogarnet series and the relationship of the series to the hydration products of Portland cement. *Journal of Research of the National Bureau of Standards* **26**, 13–33.

Gasparik, T. (1985). Titanium in ureyite: a substitution with vacancy. *Geochimica et Cosmochimica Acta* **49**, 1277–1279.

Geiger, C. A., Langer, K., Bell, D. R., Rossman, G. R. & Winkler, B. (1991). The hydroxide component in synthetic pyrope. *American Mineralogist* **76**, 49–59.

Gueguen, Y. (1977). Dislocations in mantle peridotite nodules. *Tectonophysics* **39**, 231–254.

Gueguen, Y. (1979). Dislocations in naturally deformed terrestrial olivine: classification, interpretation, applications. *Bulletin de Minéralogie* **102**, 178–183.

Guilhaumou, N., Dumas, P., Ingrin, Y., Carr, G. L. & Williams, G. P. (1999). Synchrotron infrared microspectrometry applied to petrography in micro scale range. *Internet Journal of Vibrational Spectroscopy* **3**(1), 11 (www.ijvs.com).

Gurney, J. J., Jakob, W. R. O. & Dawson, J. B. (1979). Megacrysts from the Monastery kimberlite pipe, South Africa. In: Boyd, F. R. & Meyer, H. O. A. (eds) *The Mantle Sample: Inclusions in Kimberlites and*

Other Volcanics. Washington, DC: American Geophysical Union, pp. 227–243.

Gurney, J. J., Moore, R. O. & Bell, D. R. (1998). Mineral associations and compositional evolution of Monastery kimberlite megacrysts. *Extended Abstracts, 7th International Kimberlite Conference*. Cape Town: University of Cape Town, pp. 290–292.

Harlow, G. E. (1997). K in clinopyroxene at high pressure and temperature; an experimental study. *American Mineralogist* **82**, 259–269.

Harte, B. (1983). Mantle peridotites and processes—the kimberlite sample. In: Hawkesworth, C. J. & Norry, M. J. (eds) *Continental Basalts and Mantle Xenoliths*. Nantwich: Shiva, pp. 46–91.

Harte, B. & Gurney, J. J. (1981). The mode of formation of chromium-poor megacryst suites from kimberlites. *Journal of Geology* **89**, 749–753.

Hatton, C. J. (1998). The kimberlite–megacryst link at the Monastery Mine. *Extended Abstracts, 7th International Kimberlite Conference*. Cape Town: University of Cape Town, pp. 314–316.

Hercule, S. & Ingrin, J. (1999). Hydrogen in diopside; diffusion, kinetics of extraction–incorporation, and solubility. *American Mineralogist* **84**, 1577–1587.

Hervig, R. L., Smith, J. V. & Dawson, J. B. (1986). Lherzolite xenoliths in kimberlites and basalts: petrogenetic and crystallochemical significance of some minor and trace elements in olivines, pyroxenes, garnets and spinel. *Transactions of the Royal Society of Edinburgh, Earth Science* **77**, 181–201.

Hirth, G. & Kohlstedt, D. L. (1996). Water in the oceanic upper mantle: implications for rheology, melt extraction and the evolution of the lithosphere. *Earth and Planetary Science Letters* **144**, 93–108.

Hops, J. J., Gurney, J. J. & Harte, B. (1992). The Jagersfontein Cr-poor megacryst suite: towards a model for megacryst petrogenesis. *Journal of Volcanology and Geothermal Research* **50**, 143–160.

Ingrin, J., Hercule, S. & Charton, T. (1995). Diffusion of hydrogen in diopside: results of dehydration experiments. *Journal of Geophysical Research* **100**, 15489–15499.

Ingrin, J. & Skogby, H. S. (2000). Hydrogen in nominally anhydrous upper-mantle minerals; concentrations levels and implications. *European Journal of Mineralogy* **12**, 543–570.

Irving, A. J. (1974). Megacrysts from the Newer Basalts and other basaltic rocks of southeastern Australia. *Geological Society of America Bulletin* **85**, 1503–1514.

Jakob, W. R. O. (1977). Geochemical aspects of the megacryst suite from the Monastery kimberlite pipe. M.Sc. thesis, University of Cape Town, 81 pp.

Jones, R. A. (1987). Strontium and neodymium isotopic and rare-earth element evidence for the genesis of megacrysts in kimberlites of southern Africa. In: Nixon, P. H. (ed.) *Mantle Xenoliths*. Chichester: John Wiley, pp. 711–724.

Karato, S. (1986). Does partial melting reduce the creep strength of the upper mantle? *Nature* **319**, 309–310.

Karato, S. (1990). The role of hydrogen in the electrical conductivity of the upper mantle. *Nature* **347**, 272–273.

Köhler, T. P. & Brey, G. P. (1990). Calcium exchange between olivine and clinopyroxene calibrated as a geothermobarometer for natural peridotites from 2 to 60 kb with applications. *Geochimica et Cosmochimica Acta* **54**, 2375–2388.

Kohlstedt, D. L., Keppler, H. & Rubie, D. C. (1996). Solubility of water in the α, β and γ phases of $(Mg,Fe)_2SiO_4$. *Contributions to Mineralogy and Petrology* **123**, 345–357.

Kohlstedt, D. L. & Mackwell, S. J. (1998). Diffusion of hydrogen and intrinsic point defects in olivine. *Zeitschrift für Physikalische Chemie* **207**, 147–162.

Kohlstedt, D. L. & Mackwell, S. J. (1999). Solubility and diffusion of 'water' in silicate minerals. In: Wright, K. & Catlow, R. (eds) *Microscopic Properties and Processes in Minerals*. Dordrecht: Kluwer, pp. 539–559.

Kurosawa, M., Yurimoto, H., Matsumoto, K. & Sueno, S. (1993). Water in Earth's mantle: hydrogen analysis of mantle olivine, pyroxenes and garnet using the SIMS. In: Blanchard, D. & Black, D. (chairmen) *Proceedings of the 24th Lunar and Planetary Science Conference*. Houston, TX: Lunar and Planetary Institute, pp. 839–840.

Kurosawa, M., Yurimoto, H. & Sueno, S. (1997). Patterns in the hydrogen and trace element compositions of mantle olivines. *Physics and Chemistry of Minerals* **24**, 385–395.

Lu, R. & Keppler, H. (1997). Water solubility in pyrope. *Contributions to Mineralogy and Petrology* **129**, 35–42.

Mackwell, S. J. & Kohlstedt, D. L. (1990). Diffusion of hydrogen in olivine: implications for water in the mantle. *Journal of Geophysical Research* **95**, 5079–5088.

Mackwell, S. J., Kohlstedt, D. L. & Paterson, M. S. (1985). The role of water in the deformation of olivine single crystals. *Journal of Geophysical Research* **90**, 11319–11333.

Martin, R. F. & Donnay, G. (1972). Hydroxyl in the mantle. *American Mineralogist* **57**, 554–570.

Matsyuk, S. S., Langer, K. & Hoesch, A. (1998). Hydroxyl defects in garnets from mantle xenoliths in kimberlites of the Siberian platform. *Contributions to Mineralogy and Petrology* **132**, 163–179.

Matveev, S., O'Neill, H. S., Ballhaus, C., Taylor, W. R. & Green, D. H. (2001). Effect of silica activity on OH^- IR spectra of olivine: implications for low-$a$$SiO_2$ mantle metasomatism. *Journal of Petrology* **42**, 721–729.

McDonough, W. F. (1990). Constraints on the composition of the continental lithospheric mantle. *Earth and Planetary Science Letters* **101**, 1–18.

Meade, C., Reffner, J. A. & Ito, E. (1994). Synchrotron infrared absorbance measurements of hydrogen in $MgSiO_3$ perovskite. *Science* **264**, 1558–1560.

Mercier, J.-C. C. (1979). Peridotite xenoliths and the dynamics of kimberlite intrusion. In: Boyd, F. R. & Meyer, H. O. A. (eds) *The Mantle Sample: Inclusions in Kimberlites and Other Volcanics*. Washington, DC: American Geophyisical Union, pp. 197–212.

Michael, P. J. (1988). The concentration, behavior and storage of water in the suboceanic upper mantle: implications for mantle metasomatism. *Geochimica et Cosmochimica Acta* **52**, 555–566.

Michael, P. J. (1995). Regionally distinctive sources of depleted MORB: evidence from trace elements and H_2O. *Earth and Planetary Science Letters* **131**, 301–320.

Miller, G. H., Rossman, G. R. & Harlow, G. E. (1987). The natural occurrence of hydroxide in olivine. *Physics and Chemistry of Minerals* **14**, 461–472.

Mitchell, R. H. (1986). *Kimberlites: Mineralogy, Geochemistry and Petrology*. New York: Plenum.

Moore, R. O. (1986). A study of the kimberlites, diamonds and associated rocks and minerals from the Monastery Mine, South Africa. Ph.D. thesis, University of Cape Town.

Moore, R. O., Griffin, W. L., Gurney, J. J., Ryan, C. G., Cousens, D. R., Sie, S. H. & Suter, G. F. (1992). Trace element geochemistry of ilmenite megacrysts from the Monastery kimberlite, South Africa. *Lithos* **29**, 1–18.

Neal, C. R. & Davidson, J. P. (1989). An unmetasomatized source for the Malaitan alnoite (Solomon Islands): petrogenesis involving zone refining, megacryst fractionation, and assimilation of oceanic lithosphere. *Geochimica et Cosmochimica Acta* **53**, 1975–1990.

Nixon, P. H. & Boyd, F. R. (1973). The discrete nodule association in kimberlites from northern Lesotho. In: Nixon, P. H. (ed.) *Lesotho*

Kimberlites. Maseru: Lesotho National Development Corporation, pp. 67–75.

Nowell, G. M., Pearson, G. D., Kempton, P. D., Carlson, R. W., Bell, D. R. & Zartman, R. E. (1999). Hf isotope analysis of kimberlite megacrysts by laser ablation and solution mode plasma ionization multi collector mass-spectrometry (PIMMS): evidence for a contribution from a deep mantle component in kimberlites and megacryst magmas? In: *9th Annual V. M. Goldschmidt Conference. LPI Contribution 971*. Houston, TX: Lunar and Planetary Science Institute, abstract 7398 (CD-ROM).

Paterson, M. S. (1982). The determination of hydroxyl by infrared absorption in quartz, silicate glasses and similar materials. *Bulletin de Minéralogie* **105**, 20–29.

Peslier, A. H., Luhr, J. F. & Post, J. (2002). Low water contents in pyroxenes from spinel-peridotites of the oxidized, sub-arc mantle wedge. *Earth and Planetary Science Letters* **201**, 69–86.

Poirier, J.-P. & Duba, A. (1997). On power-law kinetics of transport phenomena in minerals. *Physics and Chemistry of Minerals* **24**, 495–499.

Pouchou, J.-L. & Pichoir, R. (1991). Quantitative analysis of homogeneous or stratified microvolumes applying the model 'PAP'. In: Heinrich, K. F. J. & Newbury, D. E. (eds) *Electron Probe Quantitation*. New York: Plenum, pp. 31–76.

Rauch, M. & Keppler, H. (2002). Water solubility in orthopyroxene. *Contributions to Mineralogy and Petrology* **143**, 525–536.

Rossman, G. R. & Smyth, J. R. (1990). Hydroxyl contents of accessory minerals in mantle eclogites and related rocks. *American Mineralogist* **75**, 775–780.

Saxena, S. & Fei, Y. (1987). High pressure and high temperature fluid fugacities. *Geochimica et Cosmochimica Acta* **51**, 783–791.

Schulze, D. J. (1984). Cr-poor megacrysts from the Hamilton Branch kimberlite, Elliott County, Kentucky. In: Kornprobst, J. (ed.) *Developments in Petrology, Vol. 11B, Kimberlites II. The Mantle and Crust–Mantle Relationships*. Amsterdam: Elsevier, pp. 97–108.

Schulze, D. J. (1987). Megacrysts from alkalic volcanic rocks. In: Nixon, P. H. (ed.) *Mantle Xenoliths*. Chichester: John Wiley, pp. 433–451.

Sheppard, S. M. F. & Dawson, J. B. (1975). Hydrogen, carbon and oxygen isotope studies of megacryst and matrix minerals from Lesothan and South African kimberlites. *Physics and Chemistry of the Earth* **9**, 747–764.

Sims, K. W. & De Paolo, D. J. (1997). Inferences about mantle magma sources from incompatible element concentration ratios in oceanic basalts. *Geochimica et Cosmochimica Acta* **61**, 765–784.

Skogby, H. S. (1994). OH incorporation in synthetic clinopyroxene. *American Mineralogist* **79**, 240–249.

Skogby, H., Bell, D. R. & Rossman, G. R. (1990). Hydroxide in pyroxenes; variations in the natural environment. *American Mineralogist* **75**, 764–774.

Smith, C. B., Schulze, D. J., Bell, D. R. & Viljoen, K. S. (1995). Bearing of the subcalcic, Cr-poor megacryst suite on kimberlite petrogenesis and lithospheric structure. *Extended Abstracts, 6th International Kimberlite Conference*. Novosibirsk: Siberian Branch, Russian Academy of Sciences, pp.546–548.

Smyth, J. R. (1994). A crystallographic model for hydrous wadsleyite (beta-Mg_2SiO_4); an ocean in the Earth's interior? *American Mineralogist* **79**, 1021–1024.

Smyth, J. R., Bell, D. R. & Rossman, G. R. (1991). Incorporation of hydroxyl in upper-mantle clinopyroxenes. *Nature* **351**, 732–735.

Snyder, G. A., Taylor, L. A., Jerde, E. A., Clayton, R. N., Mayeda, T. K., Deines, P., Rossman, G. R. & Sobolev, N. V. (1995). Archean mantle heterogeneity and origin of diamondiferous eclogites, Siberia: evidence from stable isotopes and hydroxyl in garnet. *American Mineralogist* **80**, 799–809.

Sweeney, R. J., Prozesky, V. M. & Springhorn, K. A. (1997). Use of the elastic recoil detection analysis (ERDA) microbeam technique for the quantitative determination of hydrogen in materials and hydrogen partitioning between olivine and melt at high pressures. *Geochimica et Cosmochimica Acta* **61**, 101–113.

Sykes, D., Rossman, G. R., Veblen, D. R. & Grew, E. S. (1994). Enhanced H and F incorporation in borian olivine. *American Mineralogist* **79**, 904–908.

Taylor, W. R. (1998). An experimental test of some geothermometer and geobarometer formulations for upper mantle peridotites with application to the thermobarometry of fertile lherzolite and garnet websterite. *Neues Jahrbuch für Mineralogie, Abhandlungen* **172**, 381–408.

Wang, L., Zhang, Y. & Essene, E. J. (1996). Diffusion of the hydrous component in pyrope. *American Mineralogist* **81**, 706–718.

Withers, A. C., Wood, B. J. & Carroll, M. R. (1998). The OH-content of pyrope at high pressure. *Chemical Geology* **161**, 161–171.

Woodhead, J. A., Rossman, G. R. & Thomas, A. P. (1991). Hydrous species in zircon. *American Mineralogist* **76**, 1533–1546.

Wright, K. & Catlow, C. R. A. (1994). A computer study of (OH) defects in olivine. *Physics and Chemistry of Minerals* **20**, 515–518.

Wyllie, P. J. & Lee, W. J. (1999). Kimberlites, carbonatites, peridotites and silicate–carbonate liquid immiscibility explained in parts of the system CaO–(Na_2O + K_2O)–(MgO + FeO)–(SiO_2 + Al_2O_3)–CO_2. In: Gurney, J. J., Gurney, J. L., Pascoe, M. D. & Richardson, S. H. (eds) *The P. H. Nixon Volume, Proceedings of the 7th International Kimberlite Conference, Volume 2*. Cape Town: Red Roof Design, pp. 923–939.

APPENDIX

Table A1: Equations used in calculation of coexisting megacryst compositions

H_2O:		
Garnet	H_2O (ppm) = 175·8 – 1·617 Mg-number	Mg-number $\leq$74
	H_2O (ppm) = 609·3 – 7·462 Mg-number	Mg-number >74
Clinopyroxene	H_2O (ppm) = 1900·9 – 35·314 Ca-number	Ca-number >39
	H_2O (ppm) = $-37{\cdot}92 + 15{\cdot}168$ Ca-number	Ca-number $\leq$39
Olivine	H_2O (ppm) = 582·8 – 4·8874 Mg-number	Mg-number >83
Major element differentiation indices:		
From garnet	Ca-number (cpx) = $-58{\cdot}54 + 3{\cdot}535$ Mg-number$_{gt}$ $- 0{\cdot}0299$(Mg-number$_{gt}$)^2	
	Mg-number (opx) = $52{\cdot}95 + 0{\cdot}45502$ Mg-number$_{gt}$	
	Mg-number (ol) = $-141{\cdot}19 + 3{\cdot}9265$ Mg-number$_{opx}$ $- 0{\cdot}01526$(Mg-number$_{opx}$)^2	
From clinopyroxene	Mg-number (gt) = $75{\cdot}14 + 1{\cdot}0734$ Ca-number$_{cpx}$ $- 0{\cdot}0281$(Ca-number$_{cpx}$)^2	
	Mg-number (ol) = $-141{\cdot}19 + 3{\cdot}9265$ Mg-number$_{opx}$ $- 0{\cdot}01526$(Mg-number$_{opx}$)^2	
	Mg-number (opx) = $5{\cdot}40 + 0{\cdot}95502$ Mg-number$_{cp}$	
From olivine	Mg-number (opx) = $14{\cdot}67 + 0{\cdot}85128$ Mg-number$_{ol}$	
	Mg-number (gt) = $-116{\cdot}36 + 2{\cdot}1977$ Mg-number$_{opx}$	
	Mg-number (cpx) = $-5{\cdot}40 + 1{\cdot}0471$ Mg-number$_{opx}$	
	Ca-number (cpx) = 211·01 – 2·0512 Mg-number$_{cpx}$	
From orthopyroxene	Mg-number (gt) = 644·56 – 15·2908 Mg-number$_{opx}$ – 0·1004(Mg-number$_{opx}$)^2	
	Mg-number (ol) = $-141{\cdot}19 + 3{\cdot}9265$ Mg-number$_{opx}$ $- 0{\cdot}01526$(Mg-number$_{opx}$)^2	
	Mg-number (cpx) = $-5{\cdot}40 + 1{\cdot}0471$ Mg-number$_{opx}$	
	Ca-number (cpx) = 211·01 – 2·0512 Mg-number$_{cpx}$	